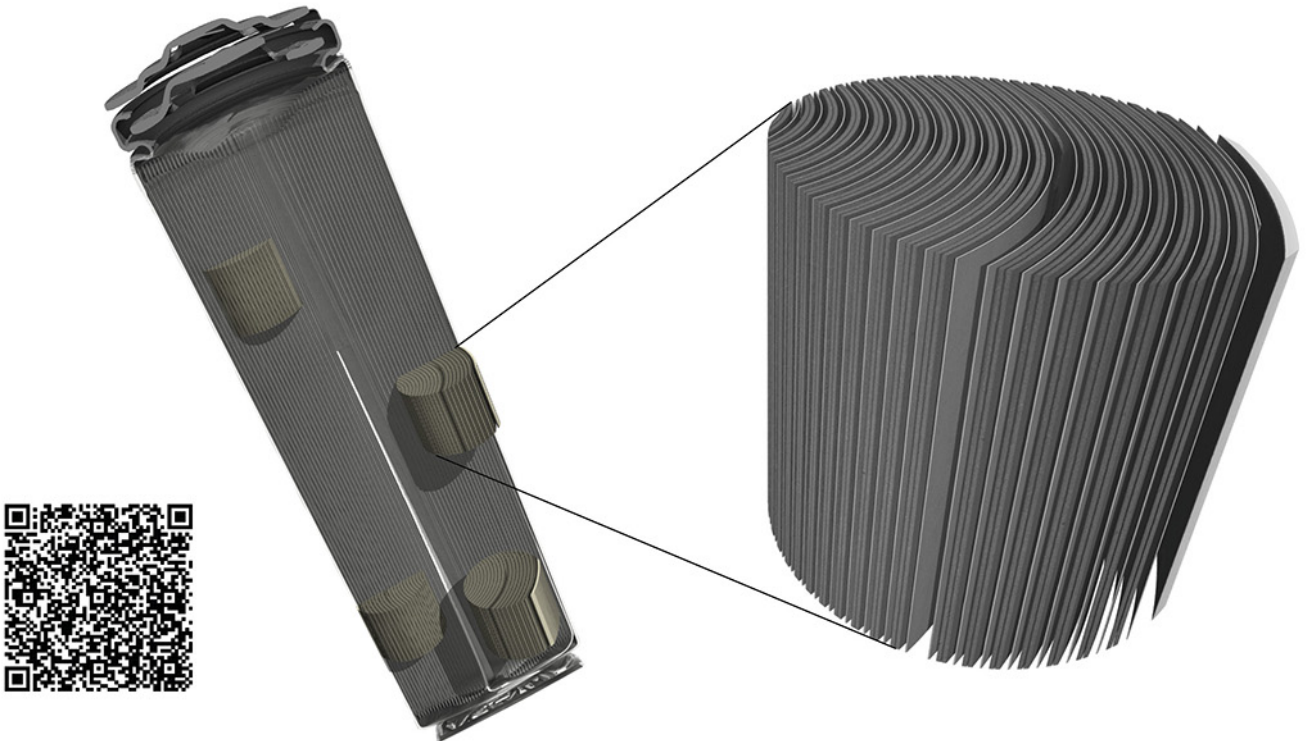# TESCAN micro-CT solutions
for energy storage materials research

TESCAN UniTOM XL

- ✓ Multi-scale non-destructive 3D imaging optimized to maximize throughput and contrast

- ✓ Fast scanning and high sample throughput with temporal resolutions below 10 seconds

- ✓ Wide array of samples types

- ✓ Enables dynamic tomography and *in-situ* experiments

- ✓ Dynamic screening for synchrotron beamtime

- ✓ Modular and open system with unmatched flexibility for research

Click and find out more

Cellulose for Light Manipulation: Methods, Applications, and Prospects

Martin Reimer and Cordt Zollfrank*

Cellulose is one of the most abundant biopolymers on earth. It is a sustainable and renewable raw material with many beneficial properties. Due to its availability, nontoxicity, environmental friendliness, biocompatibility, and biodegradability, cellulose is one of the world's most used biopolymers. Cellulose is currently establishing its role as a strong potential candidate for advanced applications in various engineering fields. In addition, cellulose and some of its derivatives exhibit properties, which recommend themselves for use in optical applications and for manipulating light in a targeted manner. In the last decades, efforts were directed toward the production of artificial ordered structures such as photonic crystals, chiral nematic liquid crystals or Bragg stacks, as well as disordered structures such as random lasers from cellulose in order to tailor the interaction of visible light with biopolymers. Due to its sustainable availability and its ability to manage light interactions, cellulose is increasingly used in optoelectronic devices to replace fossil-based polymers. Cellulose and its derivatives can be consequently applied as optical fibers, probes, organic light emitting diodes, flexible touch screens, and solar cells. The present review provides an overview of the processability and applications of cellulose and its derivatives for the specific manipulation of light.

1. Introduction

The manipulation of light is of great interest for a number disciplines, starting from biology across several physics related fields, up to material science and optical technology. Additionally, the light production as well as the manipulation is of significant importance for a variety of industrial and commercial processes and products, as detailed below.[1–9]

As so often, nature is a pioneer. When it comes to realize material applications and specific properties, we find a variety of different biological systems and materials of light manipulation used by animals or plants, which are perfected over millions of years.

M. Reimer, Prof. C. Zollfrank
Campus Straubing for Biotechnology and Sustainability
Biogenic Polymers
Technical University Munich
Schulgasse 16, 94315 Straubing, Germany
E-mail: cordt.zollfrank@tum.de

The colors of plants and animals can be achieved by different interactions of light with matter.[10–17] Animals or plants use the biological system colors as warning, for camouflage, or for signaling. Coloration can be generated by the selective absorption of light from the visible range of the spectrum by using pigments (pigmentary colors), which are absorbing subsets of the visible spectrum and transmitting and reflecting the other parts of the visible light. Therefore, the tissue occurs in the color of the wavelength of the reflected radiation. This is used for example by flowers of plants as a signal, because they have to stand out against the background of the vegetation in order to attract pollinating insects. Therefore, they appear in bright colors by reflecting certain wavelengths of visible light, which are then perceivable for the pollinating insects as well as for humans.[10–13] However, light–matter interaction with respect to absorption is of general importance, but will not be further discussed in this review.

On the other hand, coloration can be created by coherent or incoherent scattering of light on highly structured and unstructured tissues (structural colors) in the range of the wavelength of incident light. Here, different wavelengths of light are selectively reflected from a structure and the remaining wavelengths can then be transmitted or absorbed.[10–15] These biological photonic sub-micrometer structures yield a distinct coloration through the creation of a refractive index contrast between the used materials. This is an interesting fact, because natural systems cannot be built on high-refractive index inorganic materials, which are commonly used in contemporary technology. Instead, nature makes use of biopolymers such as keratin, chitin, collagen, and cellulose. However, all of these biopolymers exhibit a refractive index around ≈1.5. In order to be able to create bright structural colors, a high refractive index contrast is required. Therefore, nature is using air voids to create the necessary refractive index contrast ($\Delta n \approx 0.5$). Alternatively, nature can also use melanin with a refractive index of about 2 and keratin in mixed composites or by using anhydrous guanine with a refractive index of 1.83, whose crystal arrangements are responsible for the metallic luster of many fish.[15,16] Pigmentary color as well as structural color can also occur in combination (combined colors). All of these aspects can also be separated in iridescent or noniridescent colors.[10,15] Birds, like the Panama Amazon parrot (*Amazona ochrocephala panamensis*) or the kingfisher (*Alcedo atthis*) are using different combinations of pigments and sub-micrometer structured components.

There exists a variety of different ordered formations by using melanin, β-keratin, and air gaps to create the beautiful iridescent colors.[17] In butterflies, chitin is the main compound for the diversity of color-producing structures. The blue appearance of the *Morpho* butterfly is particularly well known here.[10,18,19] This is only a small part of the examples where nature uses structured matter for light interaction. These and other methods can act as a model to generate new materials, which influence the light specifically.[20]

In addition to the increasing trend to biomimetic approaches, the amount of natural raw materials for optoelectronic devices is also increasing.[7–9] So besides from the use of fossil-based compounds, sustainable natural materials are increasingly important because in addition to the bioeconomic perspective, the ecological impact plays an important role in modern times. The worldwide consumption of fossil raw materials and the associated emissions of carbon dioxide, as well as the contamination of land and marine areas with microplastics, make it essential to find and promote sustainable alternatives for fossil-based materials.[21,22] One of these materials is cellulose.

2. Fundamentals of Light and Cellulose

2.1. The Basic Principles of Light

In the following, the basics of light as an electromagnetic (EM) wave, techniques used for light manipulation, as well as fundamentals about the properties and the processability of cellulose for optical applications are presented in detail. Light can be considered as an EM radiation or wave. This EM wave consists of coupled electric and magnetic field components propagating in space. These electric and magnetic field vectors are oscillating transversely with an angle of 90° and are perpendicular to the direction of energy and wave propagation. The speed of light c_0 is a fundamental natural constant ($c_0 = 2.9 \times 10^8$ m s^{-1}). The main characteristics of an EM wave includes its intensity (the amplitude squared), the propagation direction, its frequency, and the polarization of the light. The frequency f is the responsible value that defines the physical properties of EM waves. Due to historical reasons, the wavelength λ is often used to describe the size of an EM wave. It describes the length of propagation the light covers in a period. The frequency f and wavelength λ are related by the speed of light ($c = f \cdot \lambda$). A spectrum describes the entirety of EM waves within a given frequency range. The spectrum of EM waves is ranging from 10^{-15} m (cosmic radiation) up to 10^7 m (high-, medium-, and low-frequency alternating currents). This includes radio waves ($\lambda > 0.1$ m), microwaves ($\lambda < 0.1$ m), infrared (IR) radiation ($\lambda < 1$ mm), visible light ($\lambda < 1$ µm), ultraviolet radiation ($\lambda < 380$ nm), X-rays ($\lambda < 10$ nm), and γ-radiation ($\lambda < 10$ pm). Only the very small frequency range between 400 and 700 nm of the spectrum is visible to the human eye. The dualistic nature of light describes that EM radiation not only behaves as a classic wave, but also as massless particle, which is called a photon. The energy of a photon is directly correlated to its frequency ($E = h \cdot f$), where h is Planck's constant.[23–25]
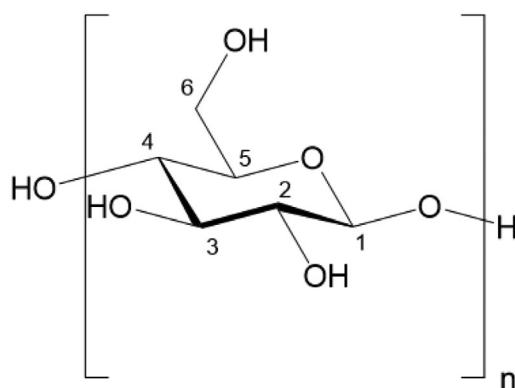
The interaction of EM waves with the array of atoms constituting a dielectric material depends on its incident frequency or equivalently on the incoming photon energy. Solid matter can interact with light by absorption, emission, transmission, reflection, refraction, and light scattering. The absorption of light occurs most visible in pigments. There, a specific wavelength of EM wave will be absorbed by the material. A pigmentary color is observed, when the energy of the wave matches the energy for the transition of an electron from the ground state to an excited level. The corresponding wavelengths are then missing in the reflected and transmitted radiation. The emission of radiation is the opposite process. There, an electron relaxes from an excited high energy state into a lower energy state and emits the corresponding energy as photon or EM wave. If there is no interaction of the incident radiation with the material, transmission occurs. Here, the beam passes through the matter without loss of energy. Reflection is a boundary surface phenomenon and describes the directional deviation of the wave propagation at an interface between two optically different media, where some of light radiation is always scattered backward. The angle of incident radiation is equal to the angle of the reflected wave in the same medium and is known as the law of reflection. The total internal reflection is a special case. Because of its importance in optical wave guiding, this will be discussed in more detail later.[23–25]

Refraction is the change of direction of the wave propagation, which passes from one medium through another medium due to the decreased velocity of light with an angle predicted by Snell's law. The ratio between the speed of light in vacuum and the speed in the medium c_M is known as the wavelength dependent refractive index n ($n = c_0/c_M$). Scattering is a general physical process in which a light beam deviates from its incident undistorted propagation direction due to localized irregularities in the medium. The light beam is deflected at scattering centers, whereby one or more new trajectories through the material as paths of wave propagation can be formed. The sum of all such scattering processes is known as diffuse scattering. If the photon carries the same amount of energy as the incident photon, it is called elastic scattering. The interaction of the incident photon with the material might involve inelastic scattering processes. As a consequence, the frequency, and thus the energy, of the photon is shifted.[23–25] These different interactions of light with solid matter can be used to analyze the optical sample properties. Optical materials can be designed in a way to control and change the light according to specific needs and considerations, which is known as manipulation of light.

2.2. Cellulose

In 1838, the French chemist Anselme Payen first mentioned a fibrous solid after treating various plant tissues with acids and ammonia and after performing an extraction procedure with water, alcohol, and ether. The term "cellulose" for the obtained plant ingredient is found for the first time in a report by the French Academy about the work of Payen in 1839.[26,27] Cellulose found its first applications as a chemical raw material around 150 years ago.[18] In 1920, the polymeric structure of cellulose was established by the research work of Hermann Staudinger. These and other discoveries of the polymeric molecular states founded the subarea of macromolecular chemistry.[27,28]

**ADVANCED
SCIENCE NEWS**
www.advancedsciencenews.com

**ADVANCED
ENERGY
MATERIALS**
www.advenergymat.de

Figure 1. Molecular structure of cellulose (*n* = DP, degree of polymerization).

Cellulose is the most abundant renewable organic raw material source on earth with a global production of ≈1.5×10^{12} tons per year. It is an essential part of the cell wall of higher plant as the basic structuring element. Cellulose can also occur alone in its pure form (e.g., in bacteria or cotton), but it is mostly surrounded by polyoses (hemicelluloses), lignin, or pectin. Cellulose has a mass fraction of 40–50% in wood, 70–80% in flax and more than 90% in cotton. In addition, several fungi and green algae, as well as bacteria of the genera *Gluconacetobacter*, *Agrobacterium*, *Rhizobium*, *Pseudomonas*, and *Sarcina* can produce cellulose, which is very pure, since they do not synthesize minor components such as lignin or hemicellulose. The cellulose is produced directly as fibrous network, with a high crystallinity and a high degree of polymerization (DP).[29] The molecular size of the cellulose is generally given as the DP. The average DP of cellulose depends on the raw material source, the type of pretreatment, and the measurement technology. The repeating unit of cellulose is the so-called anhydroglucose unit (AGU). Native cellulose has a DP varying to have 1000 and 30 000 AGUs. The chemical treatment by isolation or purification of cellulose samples can lead to depolymerization of the cellulose chain. This reduces the number of repetitive monomers that build up the rod like structure. The partial chain degradation by acid treatment or cellulase-catalyzed hydrolysis can decompose cellulose step by step until ᴅ-glucose is obtained. The molar mass of cellulose and thus the DP can be determined using viscosity measurements, size exclusion chromatography, or light scattering.[27,29]

Figure 1 shows the molecular structure of cellulose as a carbohydrate polymer. It is generated by repeating units of *β*-ᴅ-glucopyranose molecules, which are *β*-(1,4) covalently linked via a glycosidic bond. The glucopyranose rings are in an all-equatorial conformation, the $^4C_1$-chair configuration, which is the lowest energy conformation. The formation of intramolecular hydrogen bridges between to neighboring AGUs results in a linear chain structure of the cellulose.[27,29] Each AGU contains three reactive hydroxyl groups, which can be used for chemical functionalization. A primary OH-group is localized at C6 and two secondary OH-groups are found at C2 and C3. Every second AGU ring is rotated by 180° in the plane. At the ends of a cellulose chain, hydroxyl groups with different chemical properties are found. The anomeric C1-OH group at

the beginning of a cellulose molecule arises from the intramolecular hemiacetal formation and exhibits reducing properties. The C4-OH group at the end of the chain represents the non-reducing end. Due to the high proportions of OH-groups along the linear chain structure, cellulose can be readily functionalized into a variety of derivatives, e.g., ethers or esters.[27,29]

The repetitive arrangement of the hydroxyl groups within a cellulose chain leads to regular formation of strong inter- and intramolecular hydrogen bonds. This allows the founding of ordered crystalline as well as amorphous structures. These strong inter- and intramolecular hydrogen bonds, the high degree of polymerization, as well as the high crystallinity restrict the ability of cellulose to be used in many fields due to its challenging solubility. Therefore, it is essential to find and promote new solvent systems, because the cellulose cannot be dissolved in the most usual organic and inorganic solvents. The possible dissolution processes include derivatizing and nonderivatizing systems. When using derivatizing solvent systems, cellulose is dissolved by chemical interactions between the solvent and the cellulose. This leads to the formation of cellulose derivatives. These derivatives can be used as intermediates, or can be easily converted back to regenerated cellulose. Well-known derivatizing solvent systems are formic acid/zinc chloride, trifluoroacetic acid/trifluoroacetic anhydride, chlorotrimethyl silane/pyridine, nitrogen tetraoxide/dimethyl formamide, or carbon disulphide/sodium hydroxide (viscose process). By using nonderivatizing solvent systems, cellulose is dissolved by intermolecular interactions, which disrupt the hydrogen bond network and influence the supramolecular structure of cellulose only.[27,30,31] Well-known nonderivatizing solvent systems include ammonia/ammonium thiocyanate, hydrazine/thiocyanate, calcium and sodium thiocyanate, lithium chloride/*N,N*-dimethylacetamide, zinc dichloride, *N*-methyl-morpholine *N*-oxide (NMMO) monohydrate (Lyocell process), as well as aqueous alkali solution of sodium hydroxide (NaOH) such as NaOH/thiourea, NaOH/urea, or FeTNa a ferric tartraric acid complex in NaOH.[6,30–38] FeTNa can also be counted to the transition metal complex solvent systems, such as copper hydroxide/ammonia. In addition to all these special solvent systems, there is also the area of inorganic molten salt hydrates, like $LiClO_4 \cdot 2H_2O$ or $NaSCN/KSCN\text{-}LiSCN \cdot 2H_2O$.[31,39] In addition to all these solvents, there are also a large number of ionic liquids and deep eutectic solvents for dissolving cellulose.[40,41] This variety of possibilities shows that research is constantly engaging to design new solvent systems in order to be able to generate new materials with controllable properties and structures from cellulose.

The formation of hydrogen bonds between the cellulose chains leads to the generation of various crystal lattices. At least, there exist four forms of cellulose crystal structures, cellulose I, II, III, and IV of which cellulose II is considered the thermodynamically most stable structure of technical relevance. The native cellulose adopts the cellulose I modification, which consists of two allomorphs I_α and I_β, where the I_α form is compared of one-chain triclinic and the I_β form of two-chain monoclinic unit cells.[42] Both cellulose I forms have a parallel chain orientation with respect to their reducing ends and are found along the microfibrils. The relative proportions of both structures differ depending on their origin. The cellulose of

2003866 (3 of 27)

primitive organism crystallizes in the I_α phase. Whereas I_β rich specimens have been found in cotton, wood, and ramie fibers. Through dissolving and regeneration of cellulose in one of the solvent systems, the cellulose adopts the cellulose II modification. During the conversion, the direction of neighboring molecular chains exchanges, whereby an antiparallel arrangement of the chains is formed. According to the current scientific view this arrangement represents the thermodynamically most stable modification.[27,42–44]

The treatment of cellulose with liquid ammonia leads to the formation of cellulose ammonia complexes. After the evaporation of ammonia, the cellulose does not return to the original crystal lattice orientation, but instead it builds up a new modification called cellulose III. If the complex is decomposed from ammonia cellulose I, or ammonia cellulose II complex, the new crystal configuration is called III$_I$ or III$_{II}$. The conversion may involve chain slippage and the reorientation of chains. In addition to improved accessibility and chemical reactivity, the products made of cellulose III exhibit an increased softness and plasticity.[45] In 1940, Hutino and Sakurada defined cellulose IV as another polymorph by X-ray diffraction method. Cellulose IV is obtained by treating cellulose II or cellulose III with glycerine at 260 °C. However, cellulose IV is less suitable for crystallographic analysis. This makes it difficult to interpret the structure. Whether cellulose IV has an orthogonal unit cell or is simply a less crystalline form of cellulose I is still under discussion.[46,47] Both cellulose III and cellulose IV have not yet been investigated or used for optical applications, yet.

The amorphous regions can be selectively removed via acid hydrolysis of the cellulose. This allows rigid, rod-shaped crystallites to be isolated. These are known as cellulose nanocrystals (CNCs). When sulfuric acid is applied, CNCs possess negatively charged sulfate groups, allowing stable aqueous dispersions to be formed. CNCs have a general diameter of about 5 to 15 nm and lengths ranging from 100 to 300 nm. They exhibit high mechanical strength, optical transparency, and excellent dispersibility in water.[48–50] By drying a CNC suspension, these nanocrystals can self-assemble into chiral nematic liquid crystalline phases, as can be seen in **Figure 2**.[50] In this formation, the rod-like mesogens have a certain orientation order that acts as a 1D photonic crystal (PC), which twists with a characteristic
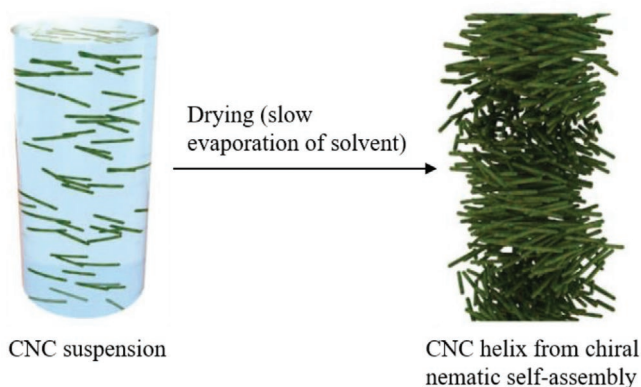
repetition distance, the pitch. This formed arrangement can produce brilliant colors when the pitch is of the order of the wavelengths of the visible light.[48,49] The pitch can be changed via various methods, allowing specific wavelengths of light to be reflected. This is explained in more detail in Section 3.1.1.

It becomes obvious from all those examples that cellulose is a very versatile biopolymer and its properties can be controlled by using suitable solvent systems and processes. This ability of cellulose and because it is the most abundant and low-cost renewable biopolymer resource available today, cellulose has gained particular attention for many applications. Cellulose is known for its nontoxicity, environmental friendliness, biocompatibility, biodegradability, thermal and chemical stability, and especially its derivatizability.[51] All of these properties make cellulose and its derivatives a versatile compound for various engineering applications as well as for the manipulation of light.

3. Photonic Structures

Tunable light sources and the management of photons are of paramount importance for information technologies and color science. Photonic materials can help here by preventing the propagation of certain wavelengths, and offer the possibility to manipulate light in a targeted manner. This can be realized by a highly ordered structure with a periodically modulated refractive index contrast.[1,52] Such materials can produce structural colors, similar to the biological structural colors of *Morpho* butterfly wings or bird feathers, and are therefore of great importance for photonic applications. Numerous photonic structures, such as chiral nematic liquid crystals, PCs and Bragg stacks have been created by using cellulose as a basic constituent.[52]

3.1. Ordered Structures

The replacement of fossil-based plastic materials by eco-friendly and biodegradable materials may be one of the most difficult challenges of our time. As cellulose is not only an inexpensive but also a biocompatible and biodegradable material, the use of cellulose and cellulose derivatives is therefore also very important in the field of photonic structures. Caligiuri et al. demonstrated the possibility of replicating microscale photonic structures and nanoscale metasurfaces by drop-casting a cellulose solution on suitable substrates.[53] The cellulose films have a high transparency in the visible range of the spectrum and a refractive index close to that of glass. Pure cellulose films are insoluble in water, which makes them ideal for the utilization for plasmonic and photonic sensing, where humid and liquid environments are common. The obtained microstructured PC cellulose films show high-quality diffractive properties after prolonged exposure to water. In addition, the obtained photonic films were fully biodegradable in soil and seawater, according to the ISO 17556 standard.[53]

3.1.1. Chiral Nematic Liquid Crystal

The lyotropic liquid crystalline character of CNCs was first discovered in 1959 by Marchessault et al.[54] This behavior

Drying (slow evaporation of solvent)

CNC suspension

CNC helix from chiral nematic self-assembly

Figure 2. Schematic illustration of chiral nematic self-assembly. Rods represent individual CNCs. Reproduced with permission.[50] Copyright 2014, NPG Asia Materials.

ADVANCED
SCIENCE NEWS
www.advancedsciencenews.com
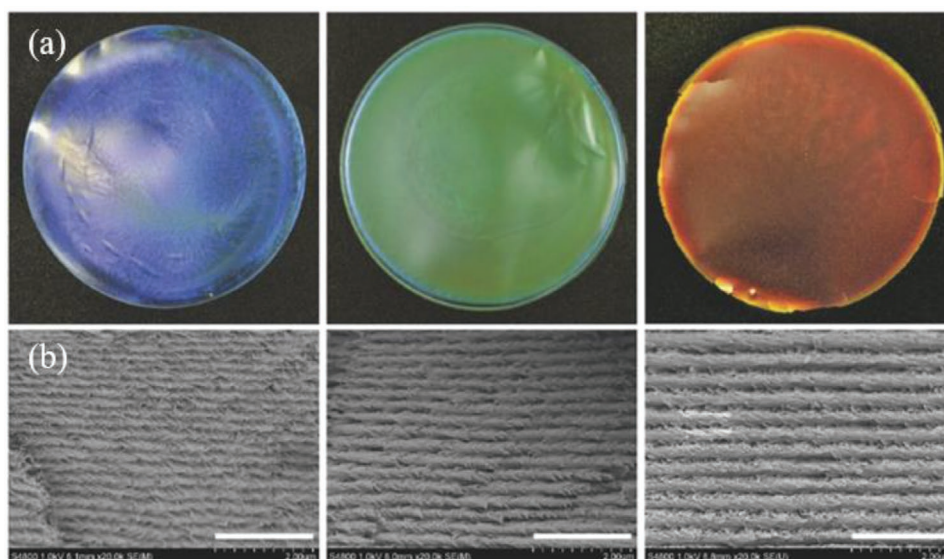
ADVANCED
ENERGY
MATERIALS
www.advenergymat.de

was later identified as a chiral nematic or a cholesteric phase by Revol et al. in 1992.[55] The molecular orientation in such chiral nematic or cholesteric liquid crystalline phases is similar to the helicoidal arrangement of microfibrils, which has been observed for cellulose in plant cell walls, e.g., *Chara vulgaris*.[56] Gray and co-workers presented the in vitro self-organization of aqueous suspensions of cellulose crystallites into stable chiral nematic phases. When the liquid of an aqueous cellulose crystallites suspension is evaporated, ordered helicoidal structures similar to biological materials can be formed.[55] This chiral nematic phase of CNC suspensions take place at a critical concentrations, between 3 and 7 wt%.[57] The proportion of CNCs used, however, has an influence on the packing order formed in the chiral nematic phase. The distances between the CNC rods in the structure decrease with increasing CNC volume fraction in the suspension. The average twist angle between two adjacent CNC rods increases from 1° to 4° when the CNC volume fraction increases from 2.5% to 6.5%.[58] The obtained chiral nematic mesostructures of the CNC films enable photonic properties. The photonic crystals have periodically changing refractive indices and selectively diffract specific wavelengths of light.[59] The reflected mean wavelength of the chiral nematic structure is influenced by the pitch (p) of the obtained helical structure, the average refractive index (n) of the substance, and the angle of the incident light ($\sin(\theta)$)[60]

$$\lambda = p \cdot n \cdot \sin(\theta) \qquad (1)$$

The helical pitch represents the length of the repeating unit for a complete 360° rotation of the axis of the mesogens. The prepared film appears in structural colors when the half of the length of pitch is in the range of the visible light. Liquid crystals have a region of reflection of circularly polarized light, where one component of the incident beam is completely unaffected.[60] The spontaneously self-assembly of CNCs forms left-handed chiral nematic structures that can be preserved upon drying. The formed chiral nematic films exhibit circular polarization properties. This includes photonic bandgap-based selective reflections. The left-handed chiral nematic structure of CNCs reflects selectively left-handed circularly polarized light and transmits selectively right-handed circularly polarized light. These optical properties arise from the left-handed chiral nematic arrangement, which is produced by evaporation-induced self-assembly from CNC suspensions at a critical concentration.[61,62] Therefore, a maximum of 50% of left-handed circularly polarized light will be reflected, and the opposite handedness transmits through the film without loss of intensity. The structural colors that is the wavelength of the reflected light can be manipulated by changing the helical pitch size of the chiral nematic structure.[57] **Figure 3** shows a biomimetic film, which mimics the coloration of the *Pollia condensata* fruit by creating a self-assembled film of cellulose-based chiral reflectors.[63] The appearance of the fruit is the effect of selective color reflection from a cellulose-based helicoidal structure in the cell wall. By influencing the pitch it is possible to imitate the structural colors produced in nature.[63]
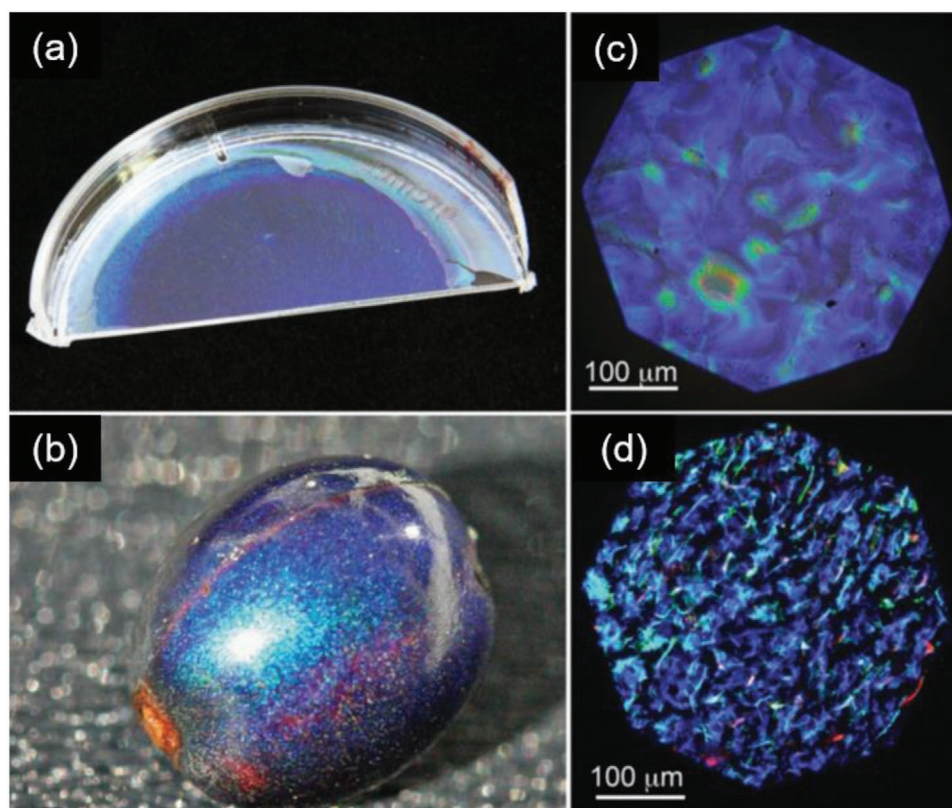
Figure 3. Biomimetic cellulose film compared with the *Pollia condensata* fruit. a) Photograph of the biomimetic film. b) Photograph of the fruit. c) Panels and d) optical microscopy images in crosspolarization configuration of the film and the fruit. Reproduced with permission.[63] Copyright 2014, Wiley-VCH.

ADVANCED
SCIENCE NEWS

www.advancedsciencenews.com

ADVANCED
ENERGY
MATERIALS

www.advenergymat.de

Figure 4. a) Photographs of CNC films with varying PEG content (PEG wt%: 10, 20, 30; film diameter of 9 cm) and b) the corresponding SEM images illustrating the changing helical pitch (scale bar: 2 μm). Reproduced with permission.[64] Copyright 2017, John Wiley & Sons.

A large number of different methods, such as changing the ionic strength of the suspension, using ultrasound, changing the drying conditions, or using magnetic or electrical fields as well as the use of different substrates on which the helical structure can be created have already been described to specifically manipulate the optical properties.[2,52,57,60–71] The distance of the helical pitch can be changed by creating a higher suspension concentration or by adding electrolytes. Increasing the electrolyte concentration, by adding HCl, NaCl, or even KCl, will reduce the electrostatic repulsion between the CNCs. This reduces the helical pitch and causes a blue-shift of the reflected light. However, the addition of electrolytes is limited. Exceeding a critical amount of electrolytes can lead to coagulation and thus to gelation or precipitation of the CNC.[57,61] The chiral nematic pitch of self-assembled CNCs in suspension can also be affected by the addition of polyethylene glycol (PEG). With increasing amount of PEG, a red-shift of the reflection peak is observed, which can be attributed to an increasing helical pitch (**Figure 4**).[64]

By applying energy via ultrasound to the nanocrystalline cellulose suspension prior to film formation, the pitch of the chiral nematic phase can be increased. As a result, the reflection band of the final iridescent film shifts to longer wavelengths. The used energy input per gram of cellulose in the sample controls the magnitude of the band shift. If suspensions with different degrees of sonication are mixed together, iridescent films are created with reflection wavelengths that correspond to the average degree of exposure. By the addition of electrolytes to the suspension, a blue-shift of reflected waves occurs. Therefore, the effects of sonication can be reversed.[2] The evaporation time of the CNC suspension also has an influence on the structure of the obtained films. A longer evaporation time leads to a reduction of the chiral nematic helical pitches and therefore to a blue-shift of the reflected wavelengths. The evaporation time is a simple parameter to influence the optical properties of the CNC films without the addition of additives.[62]

Toa et al. have shown that the ability to reflect right-handed circular polarized light by film forming at higher temperatures is possible. The ambidextrous chiroptical properties can be manipulated by changes of the evaporation temperatures. The population of nematic like domains is increased at higher temperatures during film production. They attributed this to the higher rate of solidification and concomitant reduction in fluidity during the film forming process. The amounts of the intermediate nematic-like phases increase the kinetic traps, which stabilize left-handed chiral nematic structure. Scanning electron microscopy (SEM) images confirm the absence of right-handed chiral nematic structures, which excludes the reflection from right-handed helicoids.[61]

Commercial magnets can be used to alter the orientation of cholestic domains. The generated external magnetic fields provide a powerful control to influence the CNC orientation in the suspension and therefore magnets are a good tool to adjust the photonic properties accordingly. Frka-Petesic et al. showed that simple commercial magnets like neodymium magnets influence the orientation of the formed domains and thus control the final optical properties of the resulting film.[66] The CNC suspension is vaporized in the immediate vicinity of a magnetic field, which induces a long-range order of the cholesteric phase that remains in the film. By adjusting the spatial configuration of the magnets in relation to the CNC suspension, nanostructured films with an improved uniformity of the orientation of the cholesteric axes can be produced. Thus, the intensity of the reflected light can be increased for a selected angular range. By using the magnets, the orientation of the helical structure and thus the angular optical response of the chiral nematic films can be modified.[66]

Besides the use of external magnetic fields, electric fields can also affect the orientation. By applying an alternating voltage to a CNC suspension, a homogeneous orientation of the nanocrystals can be achieved. The orientation is strongly influenced by the frequency and strength of the applied electric field. It

was observed that the orientation becomes much more homogeneous when the electric field is higher than 2000 V cm^{-1} at frequencies between 104 and 106 Hz. The manipulation is based on the interaction of the induced dipole moment and the applied electric field. A translational movement of the molecules and thus the alignment is caused by the nonuniform electric field in the solution.[67]

The photonic properties can also be modified by using different substrate surfaces. If a CNC suspension is dried on different surfaces, different iridescent colors can be produced. Depending on the polarity of the surface, varying contact angles between the liquid and the surface are formed. This results in a different thickness of the resulting film and a varied size of the pitch, depending on the polarization of the surface of the material. If a hydrophobic surface is chosen, the contact of a suspension drop is minimized, which leads to the formation of thick opaque films that resemble mother of pearl. By using hydrophilic surfaces, the suspension is spread on the substrate, resulting in the formation of thin blue colored films.[52] All these different methods can be used to change the pitch of the helical structure in order to cause specific angle dependent reflections.

In addition to the fundamental change in pitch size, the formation of an enhanced uniformity over the entire area of the film is also of great importance. It was shown that increasing the CNC concentration into the fully liquid crystalline phase as well as exposing the suspension to a circular shear flow promotes a vertical helical orientation and leads to improved uniformity.[49]

Besides these fixed iridescent colors, it is also of interest to create dynamically changing colors. In nature, many living beings can adapt their color to their environment. The cuttlefish is an example of species with vivid structural coloration, which can change their skin coloration, pattern, and texture to match with their environment for camouflage.[68] The research is focused to create smart materials to mimic this natural ability to respond to environmental changes. Anticounterfeiting trademarks, military camouflage, signaling, chemical sensing, and biotechnology represent different potential application areas, e.g., a light- and humidity-responsive chiral nematic photonic crystal film was produced.[69] The film contained cellulose nanocrystals and a photoactive polymer with hydrophilic groups (e.g., poly-(3,3′-benzophenone-4,4′-dicarboxylic acid dicarboxylate polyethylene glycol) ester). The composite forms a flexible iridescent film with a tunable chiral nematic order. The insertion of the polymer and PEG into the cellulose structure leads to a weakened intermolecular hydrogen bonds and improves the plasticity of the composite film. The sensitivity to external stimuli such as the humidity response was improved. The observed structural colors show high reproducibility, brilliant coloring, environmental friendliness, and sustainability. With increasing relative humidity, a shift in the maxima of the reflection spectra to higher wavelengths was observed. The decreased intermolecular interactions enabled an improved absorption of water and the resulting swelling. This leads to an increase of the pitch in the CNC film. Depending on the humidity, the size of the pitch increases and other wavelengths are reflected. These visual changes can also be caused by light. In addition to humidity, exposure to light can also cause a change in color. The light irradiation causes an excitation of the photoactive benzophenone groups of the polymer. The photoexcited benzophenone groups then form free radicals. The change in the pitch p is caused by structural changes in the molecule in the excited state. In the dark, the excited molecules return to the ground state. Both excitations by humidity and light are reversible processes.[69]

Another approach being pursued is the fabrication of stimuli-responsive stretchable optics. MacLachlan and co-workers report the fabrication of a homogeneous, stretchable CNC/elastomer composite with a chiral nematic structure. When subjected to mechanical stress, it deforms and the robust chiral nematic structure unwinds into a pseudonematic configuration. When stretched, the interference color changes from white to blue, yellow, pink, and green. This is a reversible process in which the material returns to its original shape after the stress is removed and the respective color disappears due to the contraction.[70,71]

3.1.2. Photonic Crystals

PCs are generated by self-assembly of colloidal particles with a periodic lattice. They can be classified into 1D, 2D, or 3D PCs. The 1D planar PCs can also be described as distributed Bragg reflectors (DBRs) and are explained in detail in Section 3.1.3.[72,73] In 2D PCs the refractive index is varied in two directions, while the 3D PCs vary the refractive index in three spatial directions (**Figure 5**). Photonic structures consist of a regular periodic structure that can inhibit isoenergetic light frequency propagation. According to the Bragg's law of diffraction, the photonic structures show brilliant color within the visible.[73] The properties depend on the structural sizes and the refractive index variations. Photonic crystals have attracted attention for applications of optical switching devices, optical sensors, displays, and packaging. A 2D colloidal monolayer of monodispersed polymethyl methacrylate (PMMA) particles was prepared by a gas–liquid interface self-assembly method. A colloidal monolayer was fabricated via a vertical self-assembly method.[1,73]

An important technical benefit of photonic crystals is the detection of various analytes. Cellulose and its derivatives can act as the surrounding solid matrix to form inverse photonic crystals, e.g., carboxymethyl cellulose can be dissolved in a methanol–water solution, and the 3D structured PMMA spheres were embedded in this carboxymethyl cellulose matrix. By etching with methylbenzene (toluene) inverse opal cellulose photonic crystal films can be generated. Different PMMA sphere diameters or different air pore sizes can be used to modify the photonic structure in order to obtain iridescent purple, blue, green, yellow, red, violet, or deep blue colors. The obtained reverse photonic crystal films exhibit a high stability, flexibility, and large specific surface area and can be used to detect different organic solvents reversibly. Therefore, the inverse opal structure was chosen as a sensing material because a single structural color detection is possible and the higher specific surface area of an inverse opal structure improves the adsorption mass transfer rate for added solutions. The organic solvents can permeate through the structure and fill up the
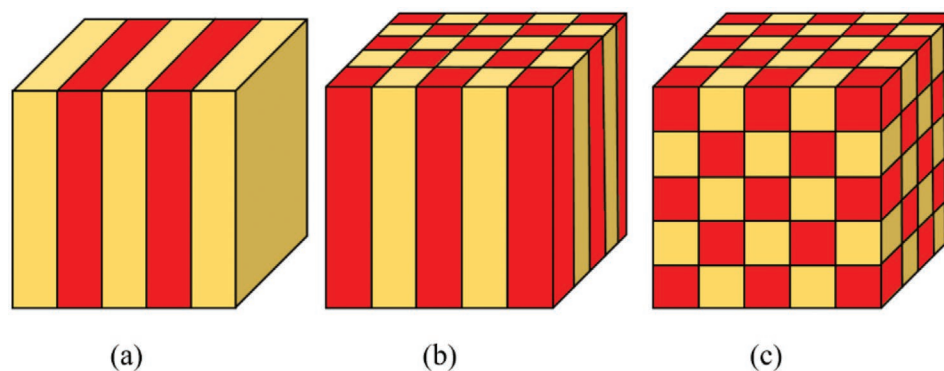
Figure 5. Schematic representation of a) 1D, b) 2D, and c) 3D photonic crystals.

air containing pores. This leads to a change in the refractive index of the photonic crystal, which in turn changes the iridescent color of the film. After removing of the solvent system, the color of the film is returning into its original appearance. Through this reversible process, such films can be used for optical switching or as in situ visual sensors.[73]

The structural color depends on the viewing angle, the used lattice distance, and the refractive index of the chosen material, e.g., a 3D hollow silica spheres photonic crystal/cellulose acetate composite film was created.[1] The hollow structure of the spheres offer a higher refractive index contrast compared to solid spheres, which enhance the brightness of the fabricated structure. The photonic crystal was created by a common dip-coating method. Hollow glass spheres are obtained by removing polystyrene (PS) core of PS@SiO$_2$ microspheres via calcination. A cellulose acetate (CA) solution was then infiltrated into the voids. After drying the composite photonic crystal film can be removed from the glass plate. According to the Bragg's law of diffraction, different colors could be obtained by using different sizes of monodisperse spheres. Therefore, reflection spectra peak positions of 555, 450, and 416 nm can be obtained after the fabrication of photonic crystals made off spheres with a size of 296, 257, and 227 nm. By using cellulose acetate for the infiltration, a colored, flexible composite film with a high mechanical stability and a high transparency was obtained. The composite film might be used for anticounterfeiting of banknotes.[1]

In addition to the self-arrangement of colloidal particles into ordered structures, as well as the formation of inverse opal matrices, ordered structures can be incorporated onto an organic material. Nanoimprinting is demonstrated as a versatile strategy that allows the fabrication of photonic crystal films, where the coloration can be changed by the imprinted structure, topology, and lattice parameters as shown in **Figure 6**.[74]

Photonic and plasmonic structures can be produced from hydroxypropyl cellulose (HPC) via moulding into submicrometric periodic lattices by using soft lithography.[74] Thus, it is possible to create biocompatible cellulose-based photonic crystals. In contrast to traditional optical lithography, the soft lithographic technique has the advantage of producing large patterned areas with high quality and reproducibility at low cost and without the necessity of working in clean rooms. Additionally, this technique is compatible with roll-to-roll processes. Espinha et al. presented a method to avoid self-assembly

of HPC by using diluted solutions to get homogenous, isotropic, and transparent unpatterned membranes. For the nanoimprinting, two different methods were used.[74] In the hot embossing technique, a hard polydimethylsiloxane stamp was slightly pressed against a heated HPC film. Another method includes the replica moulding procedure. Thereby, the cellulose
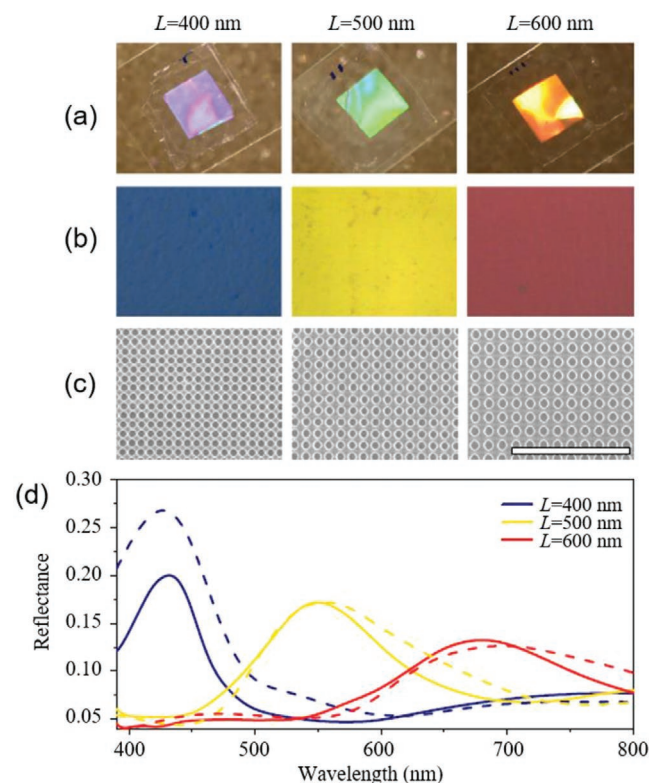
Figure 6. HPC photonic crystals. a) Photographs of the HPC photonic films, for lattice parameters of 400, 500, and 600 nm. Square lateral size is 1 cm. b) Images of the HPC photonic films acquired with an optical microscope (4× objective, NA 0.1). c) Scanning electron microscope micrographs of the HPC photonic films (top view). Scale bar: 5 µm. d) Specular reflectance characterization of the samples (solid curves), along with theoretical modeling of the structures by finite-difference time-domain calculations (dashed curves). Reproduced with permission.[74] Copyright 2018, Springer Nature.

solution was cast directly on the top of the stamp, then dried and peeled off. Both processes can produce equivalent structures. The photonic characteristics could be changed with different lattice parameters in the sub-micrometer range. The presented photonic crystals yielded iridescent colors, while retaining their material flexibility.[74] By using HPC, it is possible to produce water soluble photonic crystals, which is a good feature for environmental purposes. These processes can also be transferred to other cellulose derivatives. HPC can be crosslinked by the use of divinyl sulfone. A patterned hydrogel could then be produced using this technology, which loses its iridescence on contact with water and turns white. This is caused by the swelling of nanopores and the resulting additional light scattering. This material can be used as a fast visible moisture sensor. The use of acetyl cellulose has also made it possible to produce iridescent membranes that retain their iridescent colors in water.[74]

In plasmonic crystals, light on the surface of a metal can produce plasmonic polaritons if the condition of Bragg diffraction is fulfilled by the grating. In this way, strong electric fields on the surface of the metal can be used to intensify any light–matter interaction. These improved optical properties can be achieved by thermal evaporation of metal on top of cellulose-based gratings. Thereby the optical properties results from the combination of the photonic and the resulting plasmonic modes. Such plasmonic architectures can be used to modify and enhance the photoluminescence or surface-enhanced Raman scattering (SERS).[74] The latter increases the Raman signal significantly. Yan et al. modified an inverse methylcellulose photonic crystal with silver nanoparticles (NPs). The Raman signal is improved by the affinity of the cellulose derivative to the target analyte in organic solvents and the plasmonic responses of the silver NPs to detect analytes of low concentrations in nonaqueous solvent systems, such as industrial waste. Thus, concentrations of p-methylthiophenone up to 10^{-6} M could be quantitatively detected.[75]

3.1.3. Distributed Bragg Reflectors

The ability to control and regulate the light propagation with high precision is possible through the design of 1D DBR. These reflecting films consist of alternating different layers of dielectric materials. By changing the periodicity and the different refractive index of the materials, the fraction and wavelength of the reflected light can be influenced as can be seen in **Figure 7**. One of the major technological challenges in the production of highly reflective thin DBRs is the generation of a high refractive index contrast between the polymer layers. The majority of the currently used polymeric materials have a refractive index in the range between 1.45 and 1.65. This results in a strong limitation of the attainable refractive index contrast. There is therefore a strong interest in developing new solution methods to achieve a high selective reflection even at a lower refractive index contrast. One approach that is being pursued is the production of films with a high number of alternating layers.[76]

Multilayer highly reflective mirrors and wavelength filters are usually made with inorganic dielectric materials by methods such as vacuum evaporation and sputtering. The
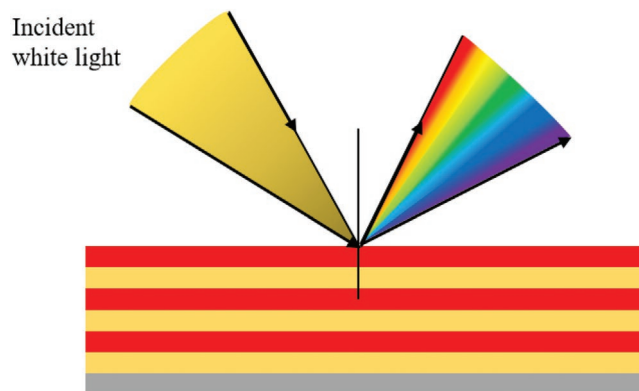
Figure 7. Schematic representation of the angular dependence of reflection for a multilayer Bragg reflector.

thickness of the individual layers can thus be controlled so that a high reflectivity is achieved when it coincides with a quarter of the corresponding wavelength. Alternatively, organic polymers can also be used for the fabrication of multilayer films. These can be constructed by self-assembly, coextrusion, or spin coating. The optical thickness of each layer can be adjusted by controlling the concentration of the polymer solution and the speed of rotation in the spin coating process. Thus, it can correspond to a quarter of the designed wavelength. An increase in the number of layers leads then to an increase in reflectivity at the designed wavelength. Poly(N-vinylcarbazole) (PVK) as high refractive index substrate ($n = 1.68$) and CA ($n = 1.475$) as low refractive index material can be used to create multilayer films with increasing reflectivity or decreasing transmissivity by increasing the number of layers as shown in **Figure 8**.[77]

If the number of layer pairs in the reflector is increased, the peaks and half-widths of the reflection band are enlarged or narrowed.[3] Another approach is to use different polymers with a higher refractive index contrast or the use of additional material repeating layers. A hyperbranched polyvinylsulfide
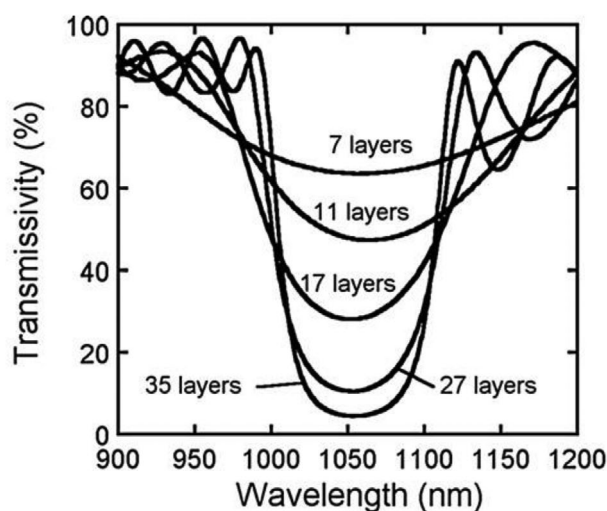
Figure 8. Transmissivity spectra of PVK:CA polymeric multilayered films for a designed wavelength of 1064 nm. Reproduced with permission.[77] Copyright 2007, Elsevier.

**ADVANCED
SCIENCE NEWS**
www.advancedsciencenews.com

**ADVANCED
ENERGY
MATERIALS**
www.advenergymat.de

polymers (HB-PVS) and CA DBR with a refractive index contrast of 0.3 was created by Gazzo et al. HB-PVS served as high refractive index material and CA as low refractive index material. A strong reflectance peak with an intensity up to 75% was obtained at a wavelength of 760 nm by creating a stack of ten bilayers.[72]

It is also possible to create high refractive index polymers via inverse vulcanization. This polymerization technique can produce polymers with a refractive index up to 2.1. Sulfur or selenium containing (co)polymers prepared via this process can be described as chalcogenide hybrid inorganic/organic polymers (CHIPs).[78] Bragg reflectors containing CHIPs with refractive index of 1.96 and CA were used to create a high refractive index contrast of 0.5. Such systems allow a high reflectance of more than 90% by using only 22 alternating layers.[76]

A seven alternating triple layer structure has been produced by using cellulose, PVA, and PVK.[79] Each layer has been obtained by covering the top surface of the substrate with a suitable polymer solution by spin coating and subsequent evaporation. As cellulose is difficult to dissolve in organic solvents and the solutions obtained cannot be spin coated easily, trimethylsilyl cellulose (TMSC) was used to build up cellulose layers. The resulting TMSC layer was then treated with hydrochloric acid vapors to regenerate cellulose. Consequently, homogenous transparent layers could be obtained. The generated structure had a reflection peak with an intensity of about 35–50% and a width of 100 nm at a wavelength of 460 nm. If the reflector is exposed to water vapor, a red-shift and a broadening of the peak occurs. Such a system can be used as a chromatic sensor for volatile polar species.[79]

Bragg reflectors can be used as selective vapor sensors. This allows the determination of volatile organic compounds without chemical functionalization. Photonic sensors based on the Flory–Huggins interaction parameter between analytes and polymer distributed Bragg reflectors can be used to detect a large amount of species with a broad selectivity without functionalizing. DBRs, which consist of alternating layers of two polymers with different refractive indices that form a dense membrane, can be used to selectively interact with the penetrating analytes for their detection via a simple estimation of the Flory–Huggins parameter. A strong reflection peak can be perceived through interaction between light and the Bragg reflector. This peak results from the coherent diffraction of the incident radiation, which then occurs at all interfaces within the multilayer. The respective reflection spectrum is influenced by varying the periodicity and the refractive index of the DBR. If a substance is stored in this multilayer, the polymer chains can swell or shrink. This changes the spacing within the photonic grating and thus the resulting reflection spectrum. The different chemical–physical affinities between the analytes and the dense membrane induce different intercalation kinetics, which can be seen in the dynamic spectrum. These kinetics are strongly related to the Flory–Huggins parameters. This allows determining the specific analyte as well as the concentration. The advantages include low production costs and simple integration in lab-on-a-chip devices, as well as large-scale established production options.[80]
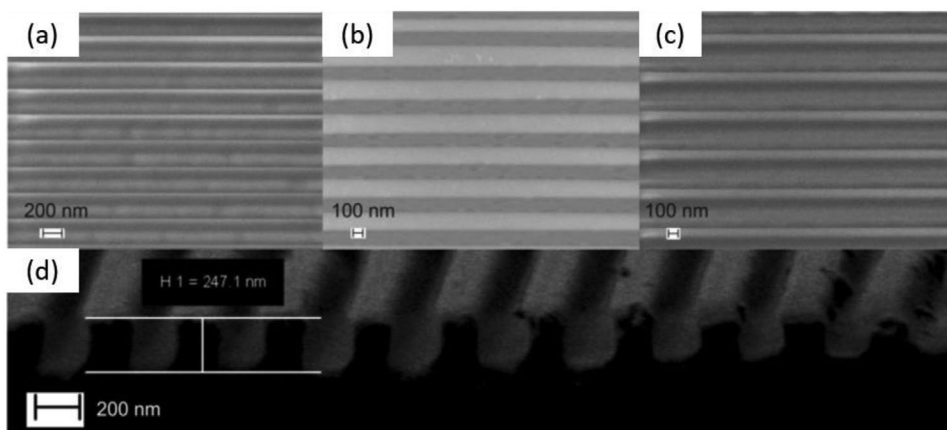
A periodic multilayer consisting of alternating inert CA and PS films modified with zinc oxide NPs ($n \approx 1.98$) was prepared by alternated spin-coating. CA acted as inert medium and the PS nanocomposite with a refractive index of 1.59 reacted as sensing medium to detect the vapor.[81]

The manufactured polymer DBRs allowed a dynamic determination of the exposure of organic vapors such as benzene, toluene, 1,2-dichlorobenzene, and carbon tetrachloride. These volatile organic compounds can cause severe damage to the human body. In the long term, exposure can cause damage to the liver, kidney and central nervous system. Such volatile gases can be released by industrial processes as well as in urban areas. Their determination is therefore of great importance. CA has a large free volume and a very good permeability to gases and vapors. Its Flory–Huggins parameter ranged from 1.2 to 2.1 for the four analytes. The permeability of PS is usually low. Through the doping with zinc oxide (ZnO) NPs, the free-volume and therefore the permeability is increased. The Flory–Huggins parameters of PS is very small for the four analytes. PS is therefore a good active material.[80]

If the DBR sensor is exposed to toluene vapor, a shift over time to longer wavelengths in the spectrum, as well as a reduction in intensity is observed. The different optical responses and spectral positions of the reflection allow the determination of the different analytes. The reflectors should show complete spectral reversibility after repeated exposure and desorption.[81]

Smirnov et al. presented the assembly of novel transparent all-polymer distributed feedback lasers. A simple and cost-effective as well as easily scalable method was suggested to generate optically high quality samples with broad transparency. Cellulose diacetate was used here as a highly transparent and flexible material substrate. Nanoimprinting can be applied to create short, medium, and long period gratings on the cellulose diacetate film. The patterned films showed additional losses, caused by diffraction, probably due to first-order diffraction at 90° on the air side of the grating. The high fidelity of the patterns on the films was verified by atomic force microscopy and SEM and grazing incident small angle X-ray scattering. It was confirmed that the pattern of the silicone master form could be transferred well and precisely onto the film as shown in **Figure 9**.[82] By spin coating, highly luminescent conjugated polymers, poly-9,9-dioctylfluorene (PFO), poly-9,9-dioctylfluorene-alt-benzothiadiazole (F8BT), and a blend of F8BT and poly(3-hexylthiophene)-poly-9,9-dioctylfluorene-alt-benzothiadiazole) (P3HT:F8BT) were deposited on the nanostructured film. This led to a perpendicular single mode laser emission in the blue, green, and red wavelength range as shown in **Figure 10**.[82] The lasing thresholds for the transparent all-polymer distributed feedback (DFB) lasers were 6.4 µJ cm⁻² for the blue, 54.0 µJ cm⁻² for green–yellow, and 6.6 µJ cm⁻² for the red emission. With pump energy fluences just above the thresholds, narrow emission peaks at 450 nm (PFO), 576 nm (F8BT), and 676 nm (P3HT:F8BT) could be detected. These peaks showed narrow linewidth values of 0.2, 0.5, and 0.3 nm. By increasing the bending angle, a progressive emission blue-shift was achieved, which was presumably caused by the decrease in the thickness of the waveguide medium. Due to the transparent structure, it is possible to stack the various DFB lasers in order to generate multicolored laser emissions.[82]

ADVANCED
SCIENCE NEWS

www.advancedsciencenews.com

ADVANCED
ENERGY
MATERIALS

www.advenergymat.de

Figure 9. Scanning electron microscope images of grating structures fabricated from cellulose diacetate films, with a) small, b) medium, and c) long period. d) Cross-section of a long period cellulose diacetate grating. Reproduced with permission.[82] Copyright 2019, Springer Nature.
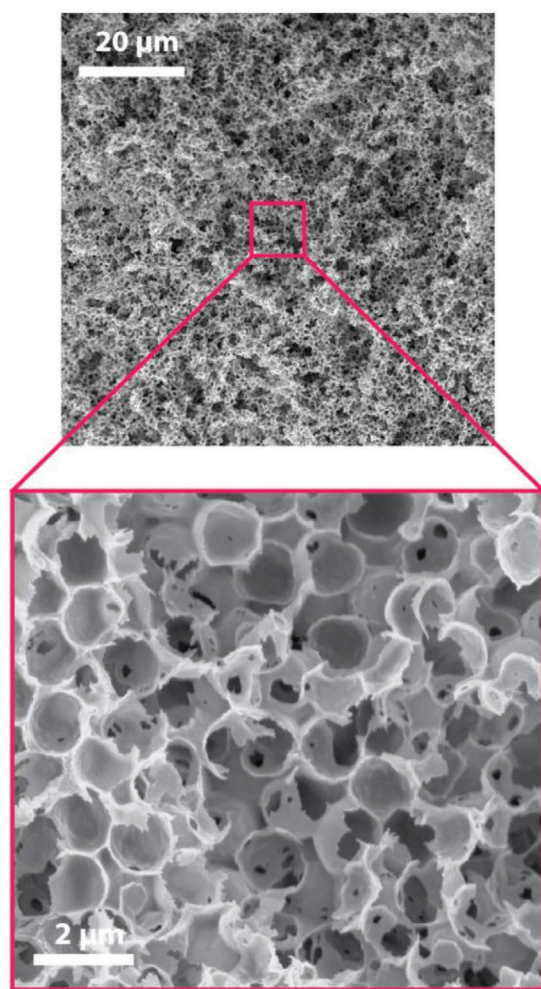
3.2. Disordered Photonic Structures

In addition to structures with a very high order, structures with a distinct or tailored disorder can also be used for the manipulation of light. In comparison to the conventional photonic structures, these do not have a specific periodic arrangement. By creating a specific degree of disorder, the light can be scattered to very high proportions to produce whiter or more opaque materials. Therefore, by a more efficient scattering, a smaller amount of material is needed to accomplish the same white coating such as the *Cyphochilus* or *Lepidiota stigma* beetle.[83]

These beetles exhibit an exceptional bright whiteness due to the mentioned multiple scattering.[84] To achieve the maximum scattering strength, a balance between scatter size, refractive index contrast, and the filling fraction is needed. A disordered cellulose-based nanostructure for enhanced light scattering was demonstrated by Caixeiro et al.[83] CNC were used as starting material to improve the light–matter interactions, due to its smaller size. A 4 wt% CNC suspension in water was mixed with colloidal monodisperse PS spheres with a diameter of 1.27 μm and filled into a hollow Teflon cylinder. The water was then removed at a slow evaporation rate. The PS spheres
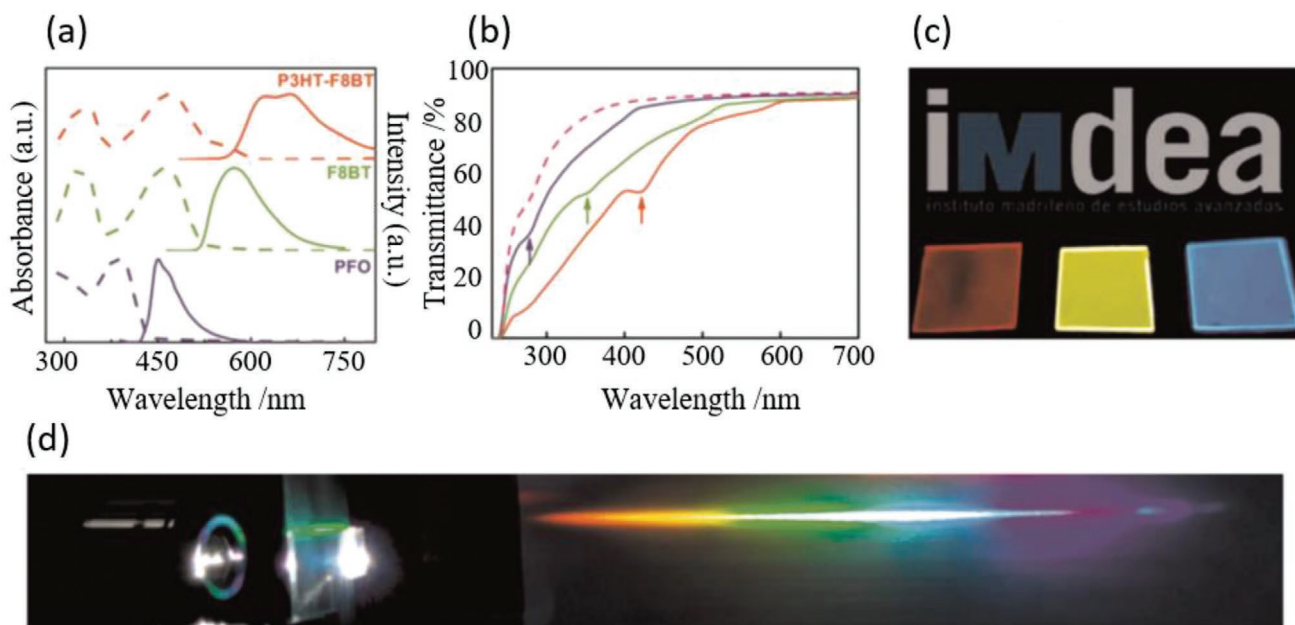
Figure 10. a) Normalized absorption and photoluminescence spectra of PFO (blue solid line and dot line), F8BT (green solid line and dot line), and P3HT:F8BT (red solid line and dot line). b) Transmission spectra at normal incidence of LP (red solid line), MP (green solid line), and SP (blue solid line) gratings imprinted on cellulose diacetate foils and of the unpatterned cellulose diacetate substrate (pink dashed line). The arrows point at the transmittance dips, corresponding to the wavelengths of 278, 350, and 416 nm, respectively. c) PFO (right), F8BT (middle), and P3HT:F8BT (left) DFB structures illuminated by a UV lamp. d) Diffraction pattern of a naked CdA grating when exposed to white light. Reproduced with permission.[82] Copyright 2019, Springer Nature.

2003866 (11 of 27)

**ADVANCED
SCIENCE NEWS**
www.advancedsciencenews.com

**ADVANCED
ENERGY
MATERIALS**
www.advenergymat.de

Figure 11. Sample morphology of a random disordered cellulose structure with micrometer-sized voids. Reproduced with permission.[83] Copyright 2017, American Chemical Society.

were subsequently removed by selective etching with toluene. This allowed the creation of a free-standing inverse photonic cellulose structure with a random tight packing arrangement (**Figure 11**).[83]

The obtained scattering response of the CNC-based photonic structure was 400% greater than that of standard cellulose fiber paper. To maximize the scattering strength for a given wavelength, it is necessary to select spheres with a diameter equal to half of the wavelength.[83]

The diffusion of light in scattering media is usually undesirable for photonic applications. However, it is necessary to differentiate between two cases: i) the scattering at ordered and ii) disordered structures. In both cases, light is scattered by inhomogeneities of the refractive index in the material, thereby electromagnetic waves will scatter with wavelengths comparable to the size of the refractive variation. If a material is present, which consists of a highly ordered structure with ordered scatterers, typically wave interference fringes are generated. These are known as Bragg diffraction. However, if the material exhibits a disordered distribution of the scatterers, the light spreads randomly in the space with a more complex

interference pattern.[85] Such a coherent multiple light scattering in a random medium, on the other hand, allows light to be trapped within the material.[86,87] This increases the photon lifetime, which in turn can be enhanced by a gain medium. Such a scattering distribution in combination with light amplification is one of the basic principles of random lasers.[86] This unique laser mechanism, is also known as feedback due to light scattering. In conventional lasers, the feedback is generated by static reflecting mirrors, whereas in random lasers it is caused by random scatterers. Random lasers opened a new perspective for partially coherent light sources.[88] Random lasers are usually simple and inexpensive devices. They consist of a random arrangement of scattering structures. These are dispersed in an optical gain medium. The optical cavities are merely represented by multiple scattering processes. A high level of precision, as in the production of ultraprecise microcavities, distributed feedback lasers or the construction of photonic crystals, is not absolutely necessary. The color and angle dependency as well as the complex features of the emission spectra can be changed in a targeted manner. The lasing threshold, which is reached when the optical gain of the laser medium is exactly balanced by the sum of all losses, can easily be modified by changing the geometry and the scattering strength of the random cavity or by tuning the gain distribution. Such a structure can be mixed with a laser dye, which acts as a gain medium. This leads to stimulated photon scattering at the random network, which in turn leads to a random laser effect, if the losses are overcome by the amplification.[89]

Nowadays, different materials can be used to create scattering media such as glass, ceramics, oxide particles, mesoporous materials, as well as cellulose-based materials.[86] In addition, various fluorophores such as dyes like rhodamine, or rare earth elements and semiconductors, as well as quantum dots can be selected as laser gain media.[86,90] Laser dyes are interesting because of their high absorption cross-section in the visible spectrum and the wide wavelength emission range. In addition, organic dyes in a solid or liquid matrix are used to generate an ultranarrow bandwidth for continuous wave laser emission. Such gain media have also been adopted in random laser applications, where the emission properties and wavelengths depend on the scattering environment. Since cellulose fibers adopt a random structuring with air cavities, photon traps are created, which allow the incident light to be randomly scattered, resulting in light amplification.[86] The random lasers can also be subdivided into nonresonant and resonant intensity feedback lasers. A nonresonant intensity feedback is characterized above the threshold by a drastic narrowing of the emission spectrum in a broad and featureless peak at the highest gain frequency. This has been realized in weakly scattering materials, with $l_t \gg \lambda$ with l_t as the transport mean free path. In addition, there are random lasers with field resonant feedback that have several sub-nanometer narrow peaks above the amplification line. This has been achieved in highly scattering systems with $l_t \geq \lambda$.[85]

Recently, it has also been shown that metal NPs can significantly increase the spontaneous emission rate in a gain medium and improve its performance. By incorporating metallic NPs into dielectric random lasers, the power is significantly improved and the threshold value is lowered due to

the improved plasmon scattering.[4,87] Metal particles, such as silver or gold particles, enable adjustable scattering properties that can be controlled by their shapes and sizes. For example, if the size of silver NPs is increased, the scattering in the spectrum shifts into the red region. In addition, changes in the shape of the particles also lead to a shift in scattering. Silver particles with a spherical shape have a scattering peak maximum at ≈400 nm, if pentagons are used, the maximum shifts to ≈500 nm. With a triangular structure, the peak maximum is shifted further into the red range to 750 nm. All shapes and the corresponding scattering are furthermore size-dependent. For triangular particles, it was additionally observed that a blue-shift is caused when the corners of the particles are changed from sharp and well defined to round. Nanorods have properties similar to those of spheres. Through the increase in length or aspect ratio, a redshift in nanorods can be generated. Nanorods are also orientation-dependent. These well-defined properties enables tunable light scattering.[5]

Using cellulose as an example, various types of random laser can be fabricated. Random lasers can be produced from suspensions, films, and electrospun fiber networks.[87,88,90,91] It is possible to construct microfluidic channels with specific architecture for random lasing, or to use cellulose sheets as biotemplate, which are then calcinated to transfer the random arrangement and structure of cellulose sheets to other materials.[85,86,89,92]

Germano et al. showed several examples using suspension and films.[90] A suspension of rhodamine 6G (Rh6G) dissolved in ethylene glycol was suspended with CNCs needles as scatterers. Here, Rh6G served as gain medium. The emission intensity could be improved by increasing the CNC concentration. The optimum emission was achieved at a concentration of 5 mg mL^{-1} CNCs in the suspension. The higher CNC concentration influenced the scattering in the medium. At 5 mg mL^{-1} CNCs the random laser efficiency improved with a threshold value of 0.35 mJ. A further increase of the concentration resulted in an increase of the threshold value, thus reducing the laser efficiency. A flexible, self-supported 70 µm thick film formed by HPC containing Rh6G and CNCs was also investigated. The film possessed a similar energy threshold like the suspension, at 10% less Rh6G and can therefore be ideally used for lab-on-chip fluorescent biosensors.[90]

By electrospinning, it is possible to produce a planar nanophotonic network from a mesh of nanoscale waveguides. Each generated structure results in a planar disordered network with a partial network topology.[91] Since it is possible to electrospin cellulose and its derivatives, this method can be applied to build a randomly structured system. Among the materials that are used as gain medium for random lasers, zinc oxide ZnO nanostructures represent a versatile alternative that can in turn interact as a scattering medium, too. A CA fiber matrix with incorporated ZnO NPs was prepared by electrospinning. This fabricated random laser structure showed a similar performance comparable to other flexible fiber-based random lasers, which predominantly use dyes as gain medium. After adding 50 nm silver nanoprisms to the matrix, the threshold energy was reduced by about 80% due to the plasmonic effect. This was caused by an enhancement of the electric field around the interface between the metallic nanoprisms and the dielectric medium, which directly benefit the ZnO emission. It is important to note that when silver particles were used, which were larger than 150 nm, no plasmonic effect was observed. The maximum of the random laser emissions occurred at a wavelength of 387 nm. The optical properties remained constant when the flexible fiber was bent. In the case of a very strong bending condition, the threshold energy increased. This is caused by the progressive decrease of the excitation intensity at the borders of the excited area compared to the center of the structure. An important advantage of using ZnO particles as gain medium is, there are in contrast to organic dyes no observable degradation effects (photobleaching) due to the interaction of the pump laser with the gain medium. The produced random laser showed a stable laser emission intensity even after 3.5×10^4 emission events.[88]

Zhang et al. proposed a plasmon enhanced random lasing in nanocomposites of highly interconnected random nanofiber networks.[87] These were directly obtained by electrospinning of a water-based HPC solution that contained gold NPs in a Rh6G gain medium. The prepared fibers had an average diameter of 260 nm with a standard deviation of 30 nm and built up a film with a variable thickness of 20 µm to 160 µm. Au NPs with 10, 40, and 80 nm were used. The color of the prepared final solution change from orange to red after mixing with increasing size of the Au particles due to the enhanced absorption in the visible range. The doped samples feature a plasmon resonance that overlap with the Rh6G emission. This significantly reduce the random lasing threshold. The scattering peak shifts from 550 to 676 nm when doped with Au NPs of increasing diameter as shown in **Figure 12**.[87]

These resonant peaks correspond to the excitation of localized surface plasmons of Au NPs embedded in the HPC matter. The measured transport mean free path was 6.78 µm in the random HPC network. After the doping with Au and Rh6G, the enhanced backscattering cone was broadened due to enhanced scattering and absorption. The random lasing threshold was reduced by 17% in the presence of 10 nm particles, compared to network only infiltrated with Rh6G dyes. By increasing the diameter particle size, the random lasing threshold also increased. Therefore it is possible to tune the localized plasmon resonance of Au NP to optimize the random lasing characteristics.[87]

Another approach for the production of random lasers is the use of microfluidic channels. These can be produced on ordinary, flexible, renewable, and biocompatible paper sheets via soft lithography without the presence of any optical cavity. The fluorescent dye can flow in the channels due to the capillarity effect. The emission properties can be controlled via the engineered fractal heterogeneity of the soft lithographically patterned disordered cellulose network. By changing the patterning processes, the width, length and shape of the paper-based microfluidic channels can be changed. The thickness of the paper determined the height of the open porous channels. The micrometer-sized channels were then filled with Rhodamine B (RhB) as a gain medium. It has been shown that if the hydraulic radius of the paper circuits is smaller than 50 µm, the threshold value is significantly reduced. It has been reported that with increasing geometric limitations, the light undergoes more scattering events that increase photon generation and
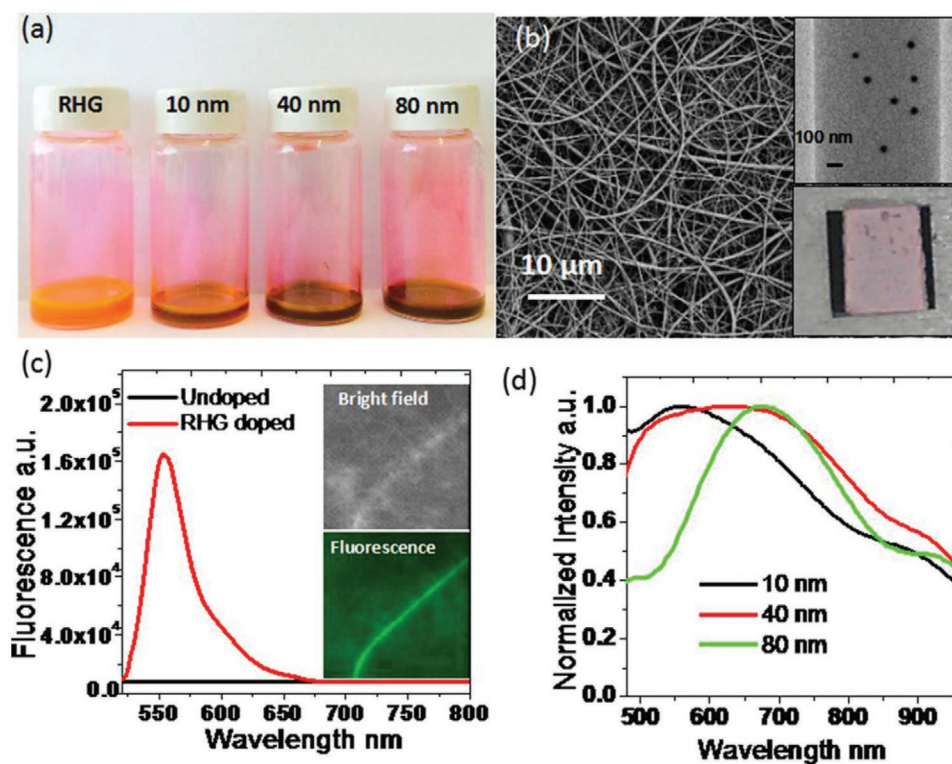
Figure 12. a) Gold NPs with 10, 40, and 80 nm and RhG6-doped HPC precursor. b) Scanning electron microscope and transmission electron microscope images of Rh6G-doped HPC nanofibers. Insets are the TEM image and a digit photo of the sample. c) Photoluminescence spectrum of undoped and Rh6G-doped nanofibers. Insets are bright-field image and fluorescence image of Rh6G-doped HPC fibers. d) Dark-field scattering spectrum of Au NPs and Rh6G codoped HPC nanofibers. Reproduced with permission.[87] Copyright 2016, AIP Publishing.
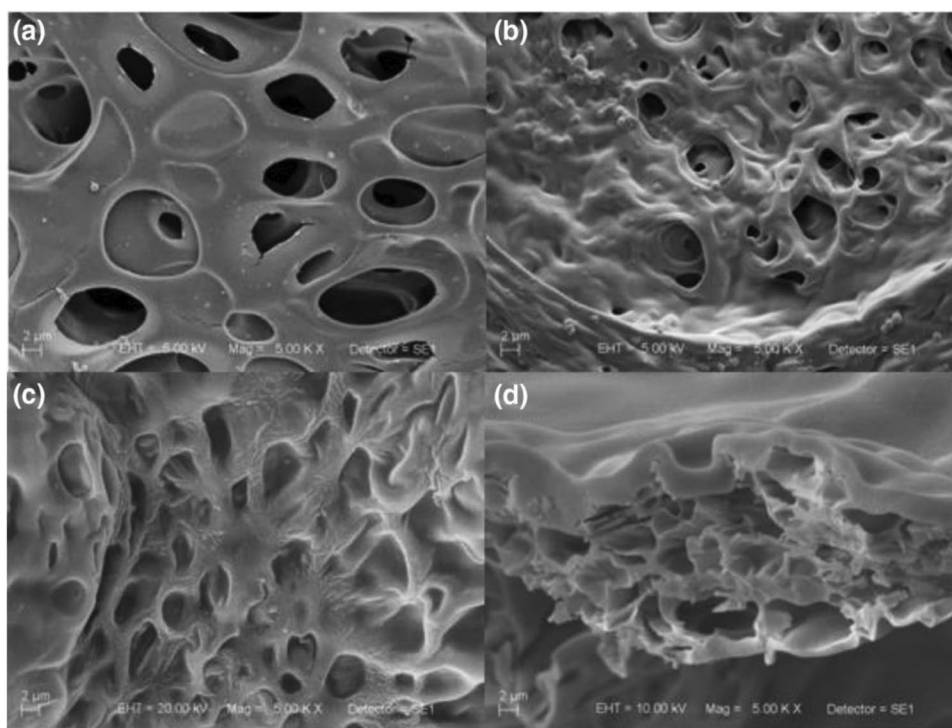
lower the threshold. With increasing geometric limitation and filling fraction, there was also a red-shift of the emission peak with a maximum at 593 nm for a hydraulic radius of 37 μm. The penetration of the microchannels with TiO_2 NPs resulted in a reduction of the threshold intensity and an increase in the random lasing peak. Therefore, the characteristics of the random laser cellulose-based paper can be changed, by varying the shape of the channels by using soft lithography.[89]

Ghofraniha et al. showed a geometry induced transition in random lasers.[85] Different microfluidic channels with a controlled width of 200, 300, and 600 μm were produced on chromatographic paper via soft lithographic techniques. RhB was chosen as gain medium. The estimated light mean transport path was ≈36 μm at 532 nm. A geometry-induced transition in random lasers has been shown. They presented random lasers where the feedback mechanism is solely given by the scattering effect when it is not confined and so called nonresonant. They also presented random lasers that are constrained in microchannels with defined walls acting as cavity that showed a laser-like behavior, caused by a secondary geometric feedback effect, which was termed as resonant random laser.[85] Cellulose networks can also be used as biotemplates. Porous regenerated cellulose can be infiltrated with an aluminoxane–epoxy–siloxane hybrid. The fiber network can then be decomposed by heating it to 600 °C. The result is a porous alumina–silica network, which adopts the former structure of the cellulose as shown in **Figure 13**. This can then be treated with a RhB ethanol solution as a gain medium to obtain a random laser.[86] Ghofraniha et al.

developed a new method to visualize and quantify the spectral and spatial patterns of the modes on a larger are sample.[92] Cellulose (filter paper) was used as biotemplate for the infiltration with tetraethyl orthotitanate (TEOT) and subsequent calcination to produce TiO_2 nanoparticles. This biomimetic structure was infiltrated with RhB as gain medium. The realized random lasers show sharp, distinct resonances with broad localization lengths, which allows the visualization and quantification of the spectral and spatial patterns of the modes on a larger area. It was shown that random modes compete for the available pump energy. Through increased pumping, some modes gain intensity and reduce their localization length at the expense of others. This is strongly dependent on the energy and width of the input laser and allows a high-resolution control of the emission characteristics by fine-tuning of the pumping parameters. The resulting information can be used to produce novel photonic functional materials.[92] Possible applications of random lasers include biophotonic applications such as fluorescence sensing, optical tagging, and detection.[87]

4. Cellulose as New Material for Optoelectronic Devices

Optoelectronics is defined as the combination of photonics and electronics, where electrons and photons are used in the same system. This synergy has the ability to generate, transport, and manipulate data at phenomenal rates. Today, it is established as

ADVANCED
SCIENCE NEWS

www.advancedsciencenews.com

ADVANCED
ENERGY
MATERIALS

www.advenergymat.de

Figure 13. Scanning electron microscope images of a) porous regenerated cellulose, b) regenerated cellulose with the hybrid dried at 60 °C, c) aluminosilicate after the thermal treatment at 600 °C, and d) side view of (c). Reproduced with permission.[86] Copyright 2019, Springer Nature.

the backbone in many sectors of information technologies.[93] Through the controllable transmittance, as well as the scattering of cellulose, a wide range of emerging optoelectronic devices can be produced by using paper-based materials. Well-known representatives of optoelectronic applications are optical fibers, sensor probes, organic light emitting diodes (OLEDs), or solar panels.

4.1. Cellulose for Light Guidance and Sensor Applications

Nowadays, the development of computer and communication technologies is still increasing. This progression of information technologies significantly facilitates the long-range exchange of information at the international and national level. The changes and further developments in communication technology play an important role in social life and create new opportunities. Therefore, fiber-optic communication methods are used to send information in the form of light from one place to another. This makes the possible interactions among individuals increasingly intense and has an important role in the information age. This further progression has led to the fact that the use of optical fibers is continuously increasing. There exist several applications for optical fibers, ranging from data transmission and sensor applications up to the illumination scenery.[94,95]

Figure 14 shows the principal process of light guidance, which is based on total internal reflection. In principle, optical fibers usually consist of a highly transparent core structure with a refractive index n_1 and a cladding with a lower refractive index n_2. If EM radiation is introduced into the fiber core

structure under a critical angle θ_{max} (acceptance angle), total internal reflection occurs at the core-cladding interface. The light beam cannot escape to the outer cladding and remains in the core. This total reflection occurs along the entire length of the fiber and can be used for waveguiding. Therefore, the radiation that hits the fiber within the acceptance cone allows transmission of EM waves. If the radiation is introduced into the fiber at a greater angle then θ_{max}, the EM radiation is no longer totally reflected at the core-cladding interface, and will be partly refracted into the cladding. There the wave is no longer unrestricted available for the signal transmission. The
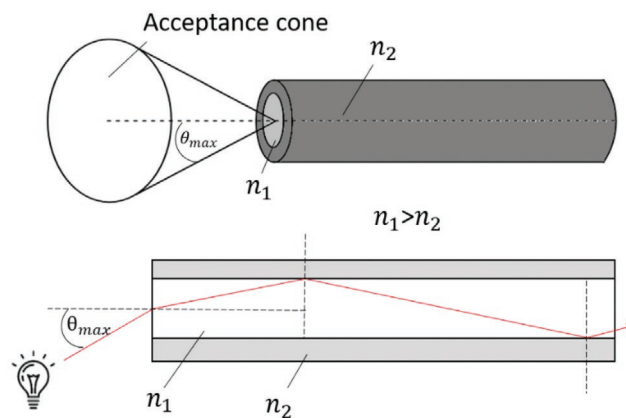
Figure 14. Principle of total internal reflection with θ_{max} as acceptance angle, and n_1 and n_2 as inner and outer refractive indices.

2003866 (15 of 27)

structure and the resulting utilization of optical fibers differs depending on the used material.[95]

Glass (silica) optical fibers are mainly used in the long-range telecommunication due to their high transmission and low attenuation loss. The best fibers made from silica exhibits an attenuation loss about 0.15 dB km^{-1} at a wavelength of 1550 nm and are building the backbone of modern telecommunication systems. In addition to their high data rate, glass optical fibers also have many disadvantages. The produced thin fibers are usually very brittle, their handling is difficult and the connection technology is rather complicated and expensive.[96,97]

In addition to these inorganic light guides, polymer optical fibers (POFs) have been developed. These consist mainly of PMMA, PS, or polycarbonate. These organic materials show transmission windows in the visible wavelength region. The attenuation loss for PMMA fibers is about 55 dB km^{-1} (538 nm), 330 dB km^{-1} (570 nm) for PS fibers, and 600 dB km^{-1} (670 nm) for polycarbonate fibers. The currently best POF fiber is an amorphous fluorinated polymer called CYTOP. It can reach an attenuation loss of 16 dB km^{-1} at a wavelength of 1310 nm. Standard step-index POFs are produced in a melt spinning process by continuous extrusion. Due to the considerable attenuation loss, POFs are generally used for short-range communication. The easy handling, flexibility and economy are the main advantages, but all commercial POFs are exclusively fossil-based. Through degradation, such materials can form microplastics, which can lead to impairment of health and the environment.[22,98]

Therefore, biocompatible as well as optionally at the end of service life biodegradable optical waveguides for photonic devices have recently gained increasing attention, particularly for special applications. The usage of biocompatible or biodegradable materials for the fabrication of optical fibers has been investigated in several scientific publications by using different materials ranging from hydrogels to synthetic polymers to natural materials such as cellulose.[99–107] The fabrication of cellulose fibers has been known for a long time (e.g., viscose and lyocell fibers). The viscose fibers are generated by dissolution of cellulose in NaOH/CS$_2$ followed by wet spinning in a coagulation bath, whereas the lyocell fibers are produced by direct dissolution in NMMO followed by dry-jet wet spinning. In both cases, these processes are well established. However, other solvents and methods can also be used.[108] In addition, transparent cellulose films can be prepared by dissolution and regeneration of cellulose. The obtained films attain a transparency up to 90% in the visible range of the spectrum.[6,109]
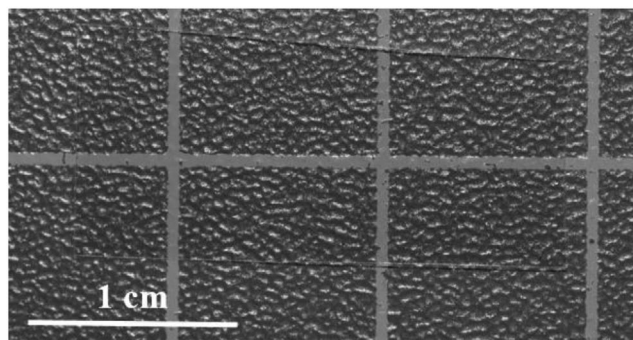
Figure 15. Highly transparent film made of regenerated cellulose by film casting method.

Figure 15 shows an obtained film of regenerated cellulose dissolved in DMAc/LiCl and regenerated by film casting method with a thickness of 54 µm.

The fabrication of fibers in combination with this optical property for the direct utilization as optical fiber is a new approach. Orelma et al. have described one of the first optical fibers made of pure regenerated cellulose for water sensor application in 2020. The core filament was prepared from dissolved cellulose in an ionic liquid (1-ethyl-3-methylimidazolium acetate [EMIM]OAc) by dry-jet wet spinning into water as coagulation medium. The cladding was prepared by using a self-made filament coater with CA. The optical fiber made of cellulose and CA transmitted light between 500 and 1400 nm. In the UV-range, the light was completely attenuated. However, Orelma et al. achieved an attenuation loss below 10 dB cm^{-1} in the range between 700 and 1350 nm and an attenuation loss limit of 6.3 dB cm^{-1} at 1300 nm. The loss limit of this biocompatible fiber was significantly higher compared to typical telecommunications fibers made from silica or PMMA. When the optical fiber made of cellulose was submerged into water, the intensity of light, which was transmitted through the fiber, decreased and the attenuation increased. When the fiber was allowed to dry, the attenuation level returned to the starting value. This show that the combination of cellulose and CA reacts sensitively to moisture and that the attenuation loss of the fiber varies due to the water absorption or desorption. Such fibers could be used as water sensor for moisture determination.[105] A further example of the versatile light guidance properties of pure regenerated cellulose from DMAc/LiCl in the visible range of the spectrum is given in **Figure 16**.

Figure 16. Light guidance through pure regenerated cellulose optical fiber.

2003866 (16 of 27)

**ADVANCED
SCIENCE NEWS**
www.advancedsciencenews.com

**ADVANCED
ENERGY
MATERIALS**
www.advenergymat.de

In addition to the use of pure cellulose, there have also been approaches for the use of cellulose derivatives, which contain cellulose esters such as cellulose butyrate, HPC, and CA. Such derivatives have already been used to produce microstructured optical fibers (MOFs) with multiple functionalities. MOFs are a new class of optical fibers and have received increasing interest in the last years due to their high potential. MOFs consist of a periodic array of microscopic air holes along the entire length of the optical fiber. Their properties depend on distribution, diameter, and the shape of the contained air holes. Holes can be filled up by air or liquids to flow through, as well as functional materials could be internally immobilized. If chemical or biological materials are filled into the holey structure, strong interaction with optical modes occur. The mechanism of sensing is based on absorption or fluorescence spectroscopy. Only small quantities of the reagents are required due to the given perforated structure. This facilitates the setup for the sensor.[110,111] Thereby, chemical sensing by using optics is under extensive research. Many optical sensors are applied in industry, environmental monitoring, medicine, or in chemical and biochemical analysis.

Such MOFs could be used for evanescent-wave-based pH sensors or ammonia gaseous and nitrite optical probes by the phenomenon of fluorescence quenching.[110–112] Therefore, a PMMA MOF with air holes can be infiltrated with a CA solution, eosin and hexadecyl trimethyl ammonium bromide (CTAB) as indicator and cationic surfactant. The eosin–CTAB–CA solution was infiltrated into the structured holes of the fiber. After the removal of the solvent, a pink colored eosin-doped CA film can be obtained. CA has a high permeability for water and ions, and eosin has a good compatibility to CA and can be used as the pH-indicator. Therefore, immobilizing surfactants on sol–gel matrices can affect the chemical and spectral properties of coentrapped pH indicators. The optical fiber was inserted into a number of pH buffer solutions and the holes were filled immediately by capillary action. A laser beam at 532 nm was placed perpendicular to the cross-section of the sample. The eosin–CTAB–CA–MPOF shows a short response time below one second. The fluorescence intensities show a linear behavior in the range from pH 1.5 to 4.5. Such optical fibers could be used for acidity detection in the human body.[110] In addition, eosin-doped CA films on MOFs were developed for gaseous ammonia fluorescence sensing. There a response time of 500 ms is needed to detect in a wide range of concentrations from 50 to 400 ppm. This represents new possibilities for optics-based gas determination.[112] If a CA solution combined with Rh6G was infiltrated into the PMMA MOF, the sample can be used for nitrite determination. Nitrites are toxic to the human body. They can react with amines into nitrosamines, which are carcinogenic. In high concentrations in blood, nitrites can change hemoglobin into methemoglobin, which has no oxygen carrier ability. Therefore, a simple, fast and selective determination is of high importance. The fluorescence quenching of the MOF can be investigated with the change of nitrite concentration in a certain concentration of sulfuric acid solution. The cause of fluorescence quenching is based on the fact that nitrites can react with Rh6G to form an *N*-nitrosamine derivative. Therefore, it was possible to determine nitrite concentrations in the range between 2.0×10^{-4} and 5.0×10^{-3} g mL^{-1}. The nitrite detection

has been demonstrated satisfactorily in real samples. The great advantage of such MOFs systems is that they only need simple chemical modifications, low required costs, and that they are easy to transfer to existing systems.[111]

In addition to the use of cellulose derivatives as a carrier matrix, they can also be used directly for the light guidance. A porous dual-core fiber structure was created with a smaller inner core of cellulose butyrate with a refractive index of 1.475. This can be either used as hollow fibers or filled with a water-soluble powder. The inner core is separated from the outer core by water soluble polydisperse HPC powder as inner cladding material with a lower refractive index of 1.337. Such a double-core structure allows efficient laser power delivery and improved collection of incoming light for passive sensing. This microstructured optical fiber could be produced by melting combined with a fiber drawing process. The glass transition temperatures of cellulose butyrate and HPC are 95 and 120 °C. Therefore, the HPC powder could be retained in a powder state during the coextrusion process by using preform structures. By controlling the withdrawal conditions, the inner core structure can be collapsed for laser delivery, or left open for potential drug delivery. The standard cutback measurement showed an attenuation constant between 1 and 2 dB cm^{-1}. By filling the inner cladding structure with water and the associated dissolution of HPC, the fiber transmission increased. This result is presumably due to the increased uniformity and reduced scattering to the side. This dual-core fiber allows for the integration of optical, microfluidic and drug release functionalities and could be used for many medical applications.[104]

4.2. Organic Light Emitting Diodes

Today, a life without the use of smartphones, televisions, tablets, desktop monitors, data projectors, or virtual reality devices is hard to imagine. It has become ubiquitous in our daily life to use at least one of these gadgets, whether for leisure or work. All these devices apply advanced display technology for the visualization of content. About two decades ago, the liquid crystal displays (LCDs) have gradually replaced the bulky and heavy cathode-ray tubes (CRTs) and have become the predominant technology. However, a LCD does not have the ability to emit and therefore requires a backlight unit (BLU) that not only increases panel thickness, but also severely restricts flexibility and the form. The subsequent development of OLEDs has led to the possibility of folding smartphones or the use of rollable televisions.[113,114] The advantages of OLEDs include a large viewing angle, high efficiency, low power consumption, and a high response speed. They are flexible, easy dimmable, are cost efficient, and exhibit a long life.[114–117]

The use of natural organic materials represents a new further development of OLEDs. The devices can be constructed entirely or only partially from natural and biological materials. This enables renewable, sustainable and possibly inexpensive organic optoelectronic devices to be produced. Such natural electronics would be biodegradable after service life or recyclable, nontoxic, and encourage environmental responsibility.[7]

Cellulose and its derivatives can be used in OLEDs as a substrate layer, as an additional diffuse layer, or as an emitting

ADVANCED
SCIENCE NEWS
www.advancedsciencenews.com

ADVANCED
ENERGY
MATERIALS
www.advenergymat.de

layer. The combination of these possibilities in a single material composite has not yet been investigated at the present time. For the use as a substrate layer, it is necessary that the produced cellulose film has a high degree of transparency. The use of cellulose in OLEDs has several advantages. The ability to achieve a high level of transparency enables the construction of conventional OLED bottom emitting structures. The use of cellulose allows a lighter construction, flexibility, and the possibility of biodegradability compared to conventional OLED substrates.[114] Purandare et al. described the fabrication of a transparent and flexible cellulose films obtained from a DMAc/LiCl solution. Therefore, a new generation of flexible OLEDs with phosphorescent emitters were produced on transparent paper with a luminance of 10 000 cd m^{-2} and emission efficiency of 47 cd A^{-1} and 20 lm W^{-1}. The obtained films had a smooth surface with a transmission of 83–86% in the visible range of the spectrum. The reconstituted cellulose film was deposited primarily with a parylene layer to inhibit gases generated during poly(3,4-ethylenedioxythiophene) polystyrene sulfonate (PEDOT:PSS) postbake from interacting with the cellulose and possible degradation. Then, a thin layer of indium tin oxide (ITO) was used as the anode. As conducting polymer PEDOT:PSS was used to enhance the hole injection capability of the anode. The OLED stack contained N,N-di-(1-naphthyl)-N,N-diphenyl-(1,1-biphenyl)-4,4-diamine as hole transport/electron blocking layer, (4,4-bis(9-carbazolyl)-1,1-biphenyl) doped with Ir(ppy)3 as emissive layer, (2,9-dimethyl-4,7-diphenyl-1,10-phenanthroline) as the hole blocking layer, and Alq3 (tris(8-hydroxyquinolinato) aluminum as the electron transport layer. A composite of aluminum/lithium fluoride served as the cathode and injects electrons into the device.[114]

Gomez and Steckl described the first approach for the construction of partially based natural OLEDs to pave the way for natural electronics or bioelectronics. In their approach cellulose serves as a natural-based alternative to glass substrates for bottom-emitting OLED structures. Cellulose was used as flexible and transparent substrate, gold as a semitransparent electrode, and the DNA base adenine served as a hole injection layer. This structure of natural materials might replace the basic structure of substrate/electrode based mostly on glass/ITO.[7]

In addition to using pure cellulose from a plant-based raw material source, bacterial cellulose was also applied. Pinto et al. created bacterial cellulose and castor oil-based polyurethane composite films for the utilization as substrate for OLEDs. These films achieve a high transmission of 90% at 700 nm and a low surface roughness about <1 nm with a good thermal stability of >250 °C.[118] Legnani et al. fabricated a multifunctional material based on bacterial cellulose and an organic–inorganic sol, composed of boehmite NPs and epoxy modified siloxane with an optical transmission of 88% as eco-friendly biocompatible substrate for flexible electronic applications.[119]

Furthermore, haze can also influence the properties in OLEDs and can be beneficially used. A porous and transparent film made of cellulose acetate butyrate was fabricated as diffuser layer on the glass substrate for green phosphorescent microcavity OLEDs. Therefore, a cellulose acetate butyrate solution was spin coated onto an OLED structure. To enhance the light-scattering effects, a 3D multistacked nanocave structure was generated by an ultrasonic humidifier method. There, water

vapor condensed on the polymer solution and formed spherical caves by sinking and drying on the surface. A unique pore structure with periodicity over the sub-micrometer scale with a small diameter and a distribution range of 300–500 nm was achieved. These nanostructures changes the optical properties such as dispersion, transmission and reflection through scattering or the occurrence of interferences. Since the pores have a size comparable to the wavelength of the visible light, the nanostructured morphology can interact with the visible light. The obtained film has a high transmittance of 94% and an optical haze of 40%. There, the haze is defined as the ratio of diffused light to the total transmitted light. As a result, these films can be used as a diffuse layer in order to redistribute the directed light from the OLEDs. This simple and cost-effective production of the porous film on an OLED reduces the viewing angle dependency of the microcavity OLEDs, but although a pixel blurring effect occurs that could ruin the resolution of the device.[120] Another possible use of cellulose in OLEDs is its utilization as an emitting organic layer. For that purpose, Shibano et al. reported the first production of thermally activated delayed fluorescence (TADF) benzyl cellulose derivatives for the fabrication of biodegradable nondoped OLEDs. These consist of carbazole as host moieties and phthalimide-based TADF dye as guest moieties. The obtained polymer was produced through ester linkages from the cellulose derivative 2,3-di-O-benzyl cellulose. This cellulose compound shows good solubility and film forming properties. The photoluminescence spectra of the spin-coated films exhibit a single emission peak, which arose from the guest moieties and indicates an efficient energy transfer from the host to the guest moieties. The cellulose film made by ratio of host and guest moieties of 97 and 7 had the highest photoluminescence quantum yields of 55.3%.[121]

4.3. Cellulose for Flexible Touchscreen Panels

A variety of electronic devices such as smart watches, mobile phones, tablets, or TVs use the function of sensing by using a touch screen. Basically, a touch screen is a computer display screen that reacts to the human touch. This allows the user to interact with the computer by selecting predefined words, images, or commands. The sensor screen is a clear transparent panel with a contact sensitive surface. The touch-sensitive area of the sensor screen covers the entire viewable area of the video screen. Several different types of sensor technologies are available, each using different methods to determine the touch input. Generally, the sensor of the screen has an electrical current or uses specific signals. By touching the screen, a change of the voltage or the signals occurs. This change can be registered and the position of the contact can be determined. Touch sensor applications have a low power consumption and a lighter weight as traditional interface devices like a standby keyboard for typing.[8,122,123] The touch sensor technologies can be fundamentally divided into four main technologies: Resistive, capacitive, surface acoustic wave, and optical touch screen.[122] Especially the latter one plays a major role in optoelectronic applications. These are using IR LED's and matching photo detectors. The basic IR touch screen consists of two IR LEDs along two adjacent sides of the screen with IR photodetectors
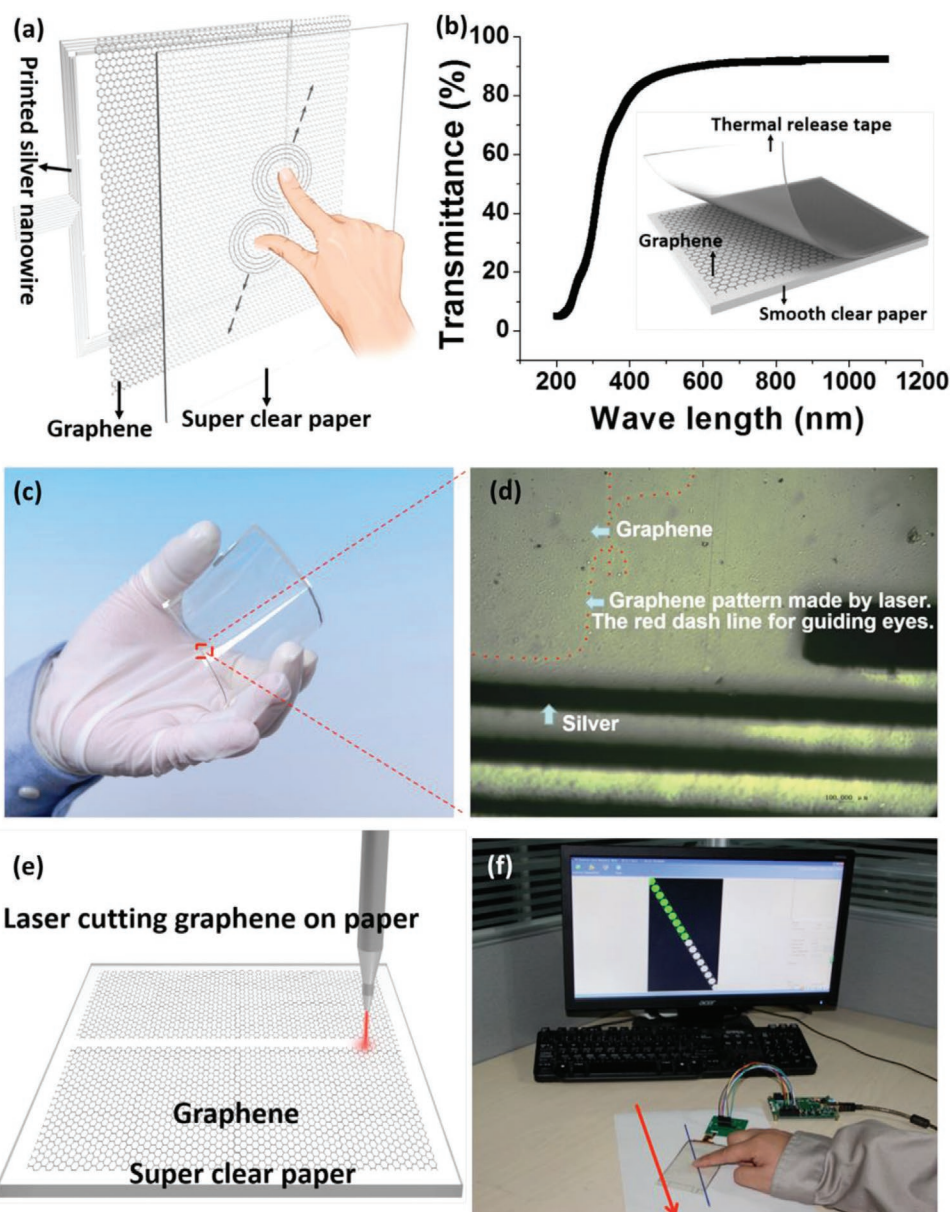
Figure 17. Transparent paper-based multitouch screen with a thin layer of graphene as a conducting electrode. a) A schematic of the paper-based multitouch screen. b) Optical Transmission of the device. c) Picture of the highly flexible, transparent paper-based touch screen. d) The zoomed-in-image to show the graphene electrodes and metal contacts patterned by laser. e) A schematic of laser cutting graphene on paper. f) Measurement of linearity of the paper touch screen. Reproduced with permission.[124] Copyright 2016, American Chemical Society.

along the other sides. The LEDs are pulsed in sequence. Through human touch, the EM wave is broken and a controller calculates the position of the contact.[122,123] The main advantages are a high optical clarity, durable surface properties, multitouch possibilities, and the device can be scaled up to large sizes. However, such devices are more expensive and the cameras might shift out of alignment.[122] For high definition displays, the optical transparency has to be very high and the haze value has to be less than 1%. Zhu et al. described an approach to generate a highly transparent and clear paper with a transmittance of 90% in the range between 400 and 1100 nm with a haze of 0.5% at 550 nm. They manipulated the light scattering

by tailoring the fiber dimensions and creating a high packing density. The generated capacitive multipoint touch screen consists of a bilayer system of transparent graphene as conductor on the highly transparent paper as shown in **Figure 17**.[124] The highly transparent paper was made of 1D cellulose nanofibers (CNFs), which exhibits excellent mechanical strength and a smooth surface roughness.[124] In another approach, a composite material based on bacterial cellulose was generated. The bacterial cellulose was prepared with grafted strontium ions at the hydroxyl positions. To improve the electroactive properties, the composite was blended with polyvinylidene fluoride. Therefore, it could be used as bendable material for touch-screen

ADVANCED
SCIENCE NEWS
www.advancedsciencenews.com

ADVANCED
ENERGY
MATERIALS
www.advenergymat.de

applications.[125] Ji et al. generated a cellulose nanofiber hybrid film, by electrospinning of an epoxy backbone and spraying cellulose nanofibers simultaneously. The hybrid film has a high transparency and low coefficients of thermal expansion. The transparent electrode layers were prepared by spin-coating silver nanowire as random networks onto the hybrid films. The hybrid films exhibit a transmittance of 83% at 550 nm and can be used on the top and bottom of transparent and flexible touch screen panels.[126]

4.4. Solar Cells

The global energy consumption is increasing enormously year by year due to rapid development, higher mobility, and the growing world population. Fossil energy sources such as coal, oil and gas currently play the leading role in covering the required energy demand. Through their consumption, the environmental pollution is constantly increasing with known disastrous consequences for the climate change. In order to protect the environment, renewable energy sources must be increasingly used. Solar energy is one of the most promising and reliable energy sources. There are several thermodynamic ways to convert solar energy into a usable form. The photovoltaic technology uses the direct conversion of solar radiation into electricity.[127] There exist various kinds of photovoltaic technologies, such as different used materials, in particular crystalline materials, thin films solar cells, hybrid solar cell, dye-sensitized solar cell (DSSC), or organic solar cells. Crystalline silicone-based solar cells play a leading role due to their high efficiency. However, cells made from crystalline materials are associated with high costs. Therefore, researchers are searching for further alternatives or improvements.[127]

The silicon solar cells are one of the most mature technologies in the photovoltaic industry today. The surface of the silicon solar cells is often partially covered by patterned gridlines. Depending on the design of the solar cell, 5–10% of the front surface can be covered. These gridlines block the incident radiation and cause shadowing losses. These losses are one of the main factors affecting the performance of silicon-based solar cells. In a simulation approach, the scattering behavior of cellulose nanocrystals in a polydimethylsiloxane polymer layer was proposed to reduce these shadowing losses. The basic idea used is highly compatible with current solar cell module manufacturing processes. Thereby, generated diffusers can provide highly efficient scattering even at a mass fraction of cellulose nanocrystals of 1%, while providing high transmissions at the same time. Simulations show that more than 30% of light could be recollected from the optical shadowing at normal incident radiation and more than 45% of the EM wave could be used at an incident angle of 60°. This leads to an increase in the efficiency with increasing angle of incidence by using cellulose nanocrystals in a polymer layer on the top of the cells.[128]
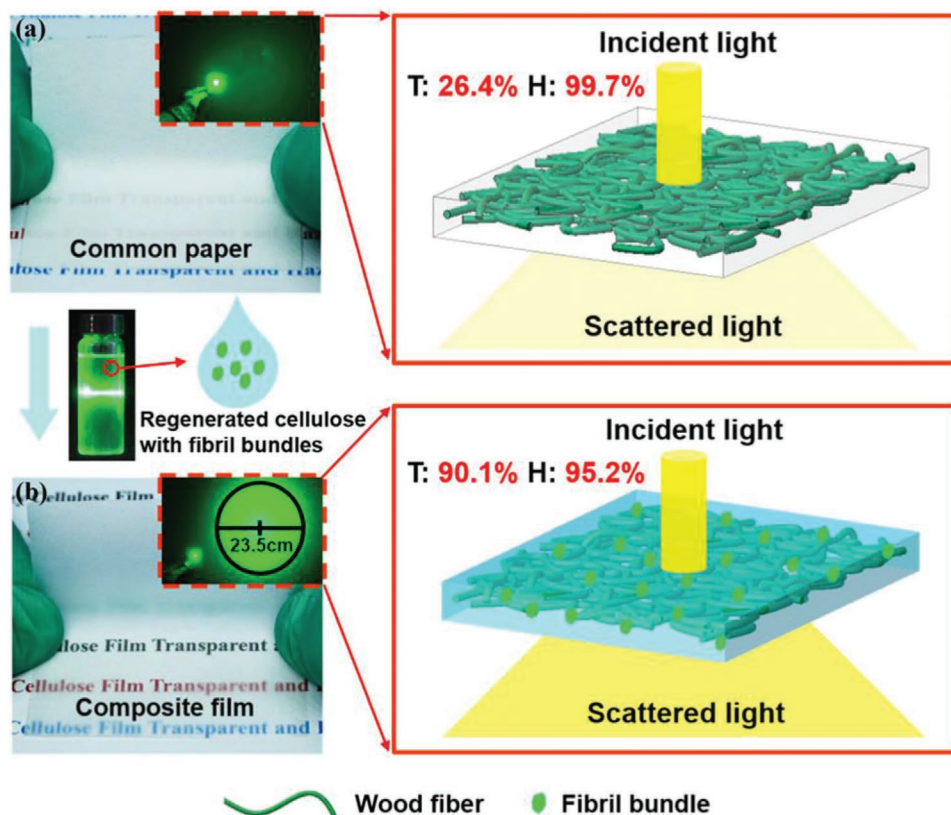
This concept was improved by combining a high optical transparency with a high haze. This was achieved by coupling the high transmission and medium haze of regenerated cellulose with a few fibril bundles and the high haze of common paper via an impregnation process. As a result, an ultrahigh

haze and highly transparent all-cellulose composite film was produced (**Figure 18**).[129] Through the combination of the different properties of the regenerated cellulose film and common paper, a transparency of 90.1% and a transmission haze of 95.2% at 550 nm was achieved. The compact composite film had a density of 0.87 g cm^{-3}, which allows an increased transmission, while microsized irregularities, caused by crystalline and amorphous regions as well as undissolved microscale nanofibril bundles in the regenerated cellulose, prefer the forward light scattering.[129]

These irregularities lead to a change in the refractive index. The refractive index of the crystalline areas was 1.584 and that of the amorphous areas was 1.532. In addition to the regions of different crystallinity, the composite material contained additional undissolved nanofibril bundles and a small number of internal cavities. Thus, there were many different interfaces in the composite film that induced intense forward scattering. The highly transparent and hazy all-cellulose composite film was used as the light management layer of perovskite solar cells. The use of the composite film improved the power conversion efficiency by 8.20%, the fill factor by 1.0%, the short-circuit current by 4.3%, and the open-circuit voltage by 2.6%, respectively.[129]

Besides crystalline materials, thin film technology and hybrid solar cells can also be used as substitutes. In principle, thin-film solar cells consist of a thin semiconductor layers that are applied to a solid carrier material. As a result of the exclusively thin films, the required amount of semiconductor material is reduced. Therefore, the required costs for the production of the corresponding modules are lowered.[130] Hybrid solar cells often consist of a combination of crystalline and noncrystalline silicon. Wu et al. proposed a photovoltaic system, which comprises amorphous and crystalline silicon in order to realize a system with a higher ratio of performance to cost.[131]

The DSSCs differ from conventional solar cells in that the function of light absorption is separated from charge carrier transport. The first device was introduced by O'Regan and Grätzel in 1991.[132] The DSSC has the advantages compared to ordinary solar cells in its low cost by using inexpensive materials and the easy way of fabrication due to the variety of suitable materials and preparation methods, for example, by using roll-to-roll processes.[133–136] Usually the electrolyte is in a liquid form, which is pumped through the cell. There, the liquid is exposed to a porous structure modified with a dye/TiO$_2$ layer. However, some additives of the electrolyte can be absorbed by this layer, which leads to an uneven distribution in the cell. This can result into a loss of efficiency of up to 35%. A proposed method to produce a uniform distribution of the electrolytes is the usage of a nanocellulose aerogel membrane made from a CNF suspension. The CNF suspension can be printed directly on the counter electrode and then freeze-dried. The aerogel serves as an absorption material for the electrolyte. After the gel is completely permeated, the cell is encapsulated. As a result, the electrolyte contacts the TiO$_2$ layer without being pumped through the cell. This prevents an irregular distribution of the additives and significantly reduces the loss of efficiency.[133] The long-term stability of this material is limited, as the cellulose nanofiber network is only held together by physical interactions. Or et al. demonstrated an alternative method of filling

**ADVANCED
SCIENCE NEWS**

www.advancedsciencenews.com

**ADVANCED
ENERGY
MATERIALS**

www.advenergymat.de

Figure 18. Schematic diagram of the structure of a highly transparent all-cellulose composite film with its haze approaching the theoretical limit. a) Opaque and hazy common paper made of intertwined wood fibers. b) Highly transparent and hazy composite film made from wood fibers and regenerated cellulose. Reproduced with permission.[129] Copyright 2020, American Chemical Society.

electrolyte in DSSCs by using aerogel films composed of covalently crosslinked cellulose nanocrystals and poly(oligoethylene glycol methacrylate) as electrolyte absorbers. These films were directly cast on transparent conducting counter electrode substrates and then used to absorb a drop-cast liquid electrolyte. The sponge like systems were stable in ACN and 3-MPN, the most commonly used solvents for DSSC electrolyte systems. This system showed similar performance and stability as the nonaerogel DSSCs and enables the production of large-area solar cell systems.[134]

The beneficial effect of nanoscale microfibrillated cellulose (MFC) was investigated by Chiappone et al. For this purpose, nanoscale microfibrillated cellulose was used in photocrosslinked polymer electrolyte membranes. Here, the MFC serves as a source for light scattering and reflection. The optical effects introduced by the cellulose improve the photocurrent, because the dye molecules are more easily reached by the photons. These quasi-solid electrolytes for the DSSC improved the sunlight conversion efficiency by up to 7.0% and 8.3% at a simulated light intensity of 1 and 0.4. In addition, the nanoscale microfibrillated cellulose showed a positive effect on the long-term stability.[135] Another dye sensitized solar cell was prepared from a starch derivative and hydroxyethyl cellulose as a binary polymer blend for use as a quasi-solid electrolyte. Thereby, a maximum photoconversion efficiency of 3.9% was achieved.[137]

From the above examples, it should become clear that the use of sustainable biopolymeric materials for advanced technical applications is highly relevant. Therefore, biobased freeze dried aerogels can be used between the electrodes of the solar cell for bearing the electrolyte.

However, natural cellulosic substrates have the disadvantage of possible contamination. These impurities, such as the remaining fragments of liginin, might reduce the efficiency by discoloration of the electrolyte. This negative effect can be avoided by using bacterial cellulose as cryogel membrane. Bacterial cellulose is especially known for its high purity. Thereby, an efficiency improvement of 44% was achieved compared to standard reference cells.[136]

Beside dye-sensitized solar cells the interest in other types of organic solar cells is currently increasing. Organic compounds such as conjugated polymers, dyes, or organic glasses exhibit semiconducting properties and high optical absorption coefficients are possible. Therefore, very thin solar cells could be prepared. An addition, the production can be accomplished on a large scale at low temperatures and at low costs.[138] In order for organic solar cells to be competitive compared to conventional silicone-based solar cells, it is necessary to achieve a power conversion efficiency of 7% reproducible on large area modules with a module lifetime of at least 5 years.[139]

Organic photovoltaic modules represent a potential economic alternative to silicon-based solar cells. They are cheaper
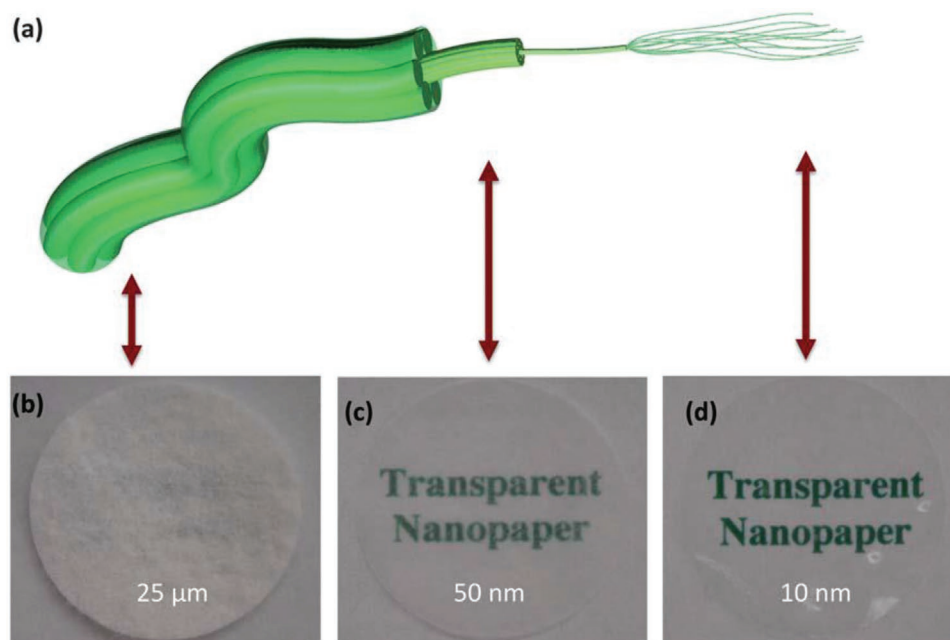
Figure 19. a) Schematic diagram of the hierarchical structure for cellulose fibers. b–d) Cellulose paper made of fibers with three different diameters, 25 mm, 50 nm, and 10 nm by same thickness of 40 mm. Visible increased transmission with smaller fiber diameter. Reproduced with permission.[9] Copyright 2013, RSC Pub.

to manufacture via solution processing, have a lower weight and are compatible with flexible materials. Conventional organic photovoltaic systems use polyethylene terephthalate, polyethylene naphthalate, or polyethersulfone as substrate. In addition to the high cost of using ITO as a conductive layer, research is interested in finding less cost intensive, recyclable or biodegradable alternatives. Cellulose might play a major role in this context.[140]

The transmission as well as the optical opacity are generally contrary in ordinary substrates. Plastics are typically highly transparent, but in most cases have only a low optical haze. Paper, on the other hand, has a high optical haze, but a low transmission. It has been shown that the combination of plastic and paper can produce both high transmission and high optical haze. Such plastic paper can provide many advantages in optoelectronic devices. In solar cell systems, the use of plastic paper can improve the wide-angle scattering, which leads to an increase of light absorption in the module and an improvement of the coupling length in solar cells. This can lead to a 15% increase in power conversion efficiency in solar cells.[141]

The use of cellulose nanomaterials is becoming increasingly important. Cellulose nanomaterials include CNF with a diameter of 4–20 nm and a length of over 1 µm, as well as CNC with a diameter of 3–10 nm and a length of 50–500 nm. A recyclable organic solar cell consisting of CNC was recently presented.[142] A film was made from CNC combined with glycerol to make the substrate more flexible. The solar cell produced exhibit a power conversion efficiency of 2.7%. The transmission represents a slight challenge here, because of the random distribution of CNC in the film. The refractive index inhomogeneities over areas with dimensions in the same order of magnitude as the wavelength of the visible light caused light scattering and therefore a decrease of transmittance.[142]

In another approach, the use of nanopaper is pursued. It is a flexible, transparent, and renewable material, which has ideal properties for green electronics. In addition to sustainability aspects, paper substrates have better properties for roll-to-roll printing. In the case of fossil-based substances, extra additives have to be compounded, which means that pure cellulose paper attracts greater attention for the production of flexible electronics.[9,143,144] Cellulose wood fibers have a unique hierarchical structure with a remarkably wide range of mechanical properties.[145] The large softwood fibers have a diameter of 20 to 40 µm and consist of many smaller fibers. These microfibrils are composed of many smaller elementary fibrils.[9,145–147] In conventional paper, the cellulose fibers have an average diameter of about 20–25 µm. At this size, there is an increased scattering of light, which makes the substrate appear opaque. In addition, a rough surface with a peak-to-valley roughness values of up to hundreds of micrometers is created, which is not suitable for electronic components. To overcome these problems, nanopaper made from cellulose nanofibrils with a cross-sectional diameter of ≈4 nm can be created. Such nanopapers are providing excellent mechanical properties with a good optical transparency and a smooth surface.[9,148] Compared to normal paper, nanopaper has a significantly increased transparency. This is based on the small size of the fiber diameter, as shown in **Figure 19**. It has a considerably smaller size than the wavelength of the visible light and therefore significantly reduces light scattering. By using nanofibers, the back-scattering effect is largely decreased. Each nanofiber will lead to a small forward scattering. Therefore, this results in a highly transparent substrate with a large scattering in the forward direction.[9,148] The cellulose fibers can be decomposed into smaller sizes by a combination of mechanical and chemical treatments. These fibers

**ADVANCED
SCIENCE NEWS**

www.advancedsciencenews.com

**ADVANCED
ENERGY
MATERIALS**

www.advenergymat.de

could be further oxidized with 2,2,6,6-tetramethylpiperidine-1-oxyl (TEMPO), a highly selective oxidant for hydroxymethyl groups at the glucose C6 position followed by a microfluidizing treatment to obtain nanofibrillated cellulose. Nanopaper can then be formed by high-pressure processes.[9] It has been shown that transmission and haze depend on the diameter of the used fibers as well as on the packing density. If the fiber diameter is much smaller than the wavelength of visible light, the scattering cross-section decreases strongly with the fiber diameter. Therefore, the basic structure size is reduced from micrometers to a few nanometers, so that the amount of scattered light is small and predominantly directed forward. This leads to a higher transparency with decreasing diameters.[9,148]

Films made of MFC fibers with a diameter of 50 or 10 nm can achieve a similar transmission of 92–93%. However, it can be noticed that the scattering of light increases in the orders of magnitude with increasing fiber diameter. Fibers with a diameter of 10 nm exhibit a haze of 20% at 550 nm, and of 49% at a diameter of 50 nm. Therefore, fibers with 50 nm are more suitable for the use in solar cells, because with a higher degree of forward scattering, the optical length and thus the light absorption in the active layer of the solar cells are increasing. Films made out of 10 nm fibers are more suitable for indoor displays, where a higher transparency is required. In addition to the fiber diameter, the packing density also plays an important role in order to be able to set the transmission and the haze. When an EM wave or a photon hits matter, interactions such as reflection, adsorption, or refraction occur. The way of interaction depends on the wavelength of the light as well as the properties of the material. A nanopaper contains internal air-filled cavities and a large-scale nonuniformity. The photon can therefore be scattered at the interfaces of these pores, where the refractive index between air and medium changes, or can be scattered internally. This means that the air in the inner pores increases the light scattering and reduces the transmittance. Therefore, if the packing density increases, the porosity of the paper will decrease. Consequently, scattering is decreased, while the transmission is enhanced.[9] Besides using cellulose as a transparent substrate, it can also be used as a top electrode through combination with graphene nanoplatelets. La Notte et al. presented a method in which all layers of the solar cell were produced by a spray process. A power conversion efficiency of over 3% was achieved.[149] All of the examples mentioned show that cellulose is increasingly important for solar energy systems and that cellulose can be used here in a variety of forms and applications.

4.5. Future Directions: Optical Trap Display and Photovoltaic Fabrics

The display technology is not only limited to the visualization of images and videos on screens of TVs, smartphones, smartwatches, and other devices. There is also a continuous research effort to break through these 2D limitations and thus to create images in 3D free space. This technology, known from science fiction novels or movies, is already possible to a limited extent at present. A currently developing technique is the optical trap display (OTP). With the use of such displays, illuminated pixels are generated in space, which makes it possible to create images in the air that can be seen from almost any direction and are not subject to clipping. For this purpose, it is necessary to levitate very fine particles. This can be achieved by different methods.[150,151] One approach being investigated is photophoretic force on particles. In an OTP based on this technique, a micrometer-sized opaque particle is trapped by a photophoretic optical trap. The trapping locations are formed by a combination of oblique astigmatism and spherical aberration. After a particle is captured, the trap is scanned and the particle is moved in volume in space. A laser system is then used to illuminate the free-floating particle, resulting in the scattering and creation of levitating pixels. The sum of individual pixels leads to the creation of free-standing 3D images with a large color scale and fine details in space, e.g., black liquor, which is a byproduct of the paper manufacturing process, can be used in the creation of such images. The liquor is a solution that contains cellulose next to other compounds with a solids content of about 70%. To the present, only proof-of-concept demonstrations of full-color, high-resolution, free-space volumetric displays using cellulose to show few-centimeter images are known.[150] The current capabilities are limited by the quality of the used traps, the variation of the particles in terms of uniformity of size and variation of particle shape, and by the speed of the scanning system. For the development of the next generation of OTD devices, trapping, scanning, scaling, as well as robustness and safety must be improved to make this technology accessible in the future.[152]

In addition to the conventional application possibilities in photovoltaic systems, there are also other new aspects where cellulose in particular might play a dominant role. Since the intense use of cell phones and tablets and other electronic devices has become a matter of course, research is now also directed toward integrating these types of technologies into textiles. Modern communication and computing tools are being transformed into portable electronics, also known as smart textiles. The first kinds of these textiles are already commercially available today. There exist, for example, snowboarding jackets, which are designed to play music files with the help of controls stitched onto the sleeves. However, the field of smart textiles is not limited to such simple functions, it can find advanced applications in medicine, advertising, as well as protective applications.[153]

Portable devices generally require electrical energy. One way to solve this energy supply is the use of rechargeable batteries. However, their storage capacity is limited, and an increasing of capacity can only be achieved on the expense of a weight increase. Another way to supply energy is energy conversion. In this process, movement, body heat and light can be used. When using light, the concept of photovoltaic systems can be transferred to the structure of fibers. These fibers can then be sewn into the fabric. A proof-of-concept for the simple production of such photovoltaic fibers was recently presented.[154] Ordinary hollow industrial viscose fibers were used for this purpose. For the other materials, only those were used that are also applied in conventional planar organic solar cells. The presented photovoltaic fibers showed remarkable properties with fill factors and short circuit current densities comparable to planar devices of this configuration. The open-circuit voltage shows a significant weakness. These losses are caused by considerable amounts of leakage current as a consequence of the inhomogeneous

covering of the semiconductor surface. However, the proof-of-concept demonstrated that a simple production of photovoltaic fibers via dip-coating, spraying or printing is possible. This type of approach shows that a simple and continuous power supply in smart textiles is possible without the use of weight-increasing batteries.[154]

5. Summary

Through the continuous development of new processing methods for cellulose and its derivatives, the possibility of manipulating light through such biopolymeric compounds is constantly increasing. Photonic structures such as photonic crystals can be created by using cellulose and its derivatives as surrounding matrix to form inverse opals, or by nanoimprinting. The self-assembly of CNCs leads to form chiral nematic liquid crystals. By changing the helical pitch, the wavelength of the reflected light can be manipulate in a targeted manner. To control and regulate the light propagation with high precision, Bragg stack can be formed by alternating layers of compounds. Disordered cellulose-based structures can be used to create random lasers. Therefore, coherent multiple light scattering in combination with light amplification can lead to a new perspective for coherent light sources. Cellulose and its derivatives can be used to create materials with a high transmission. By incorporation of CNCs or microfibrils, the scattering properties can be controlled und used in optoelectronic devices. Therefore, biopolymer optical fibers, probes, organic light emitting diodes, flexible touch screens, or solar cells with adjustable properties can be produced. This offers the unique opportunity of replacing fossil-based polymers in optoelectronics in the future and on the long term.

Acknowledgements

Conflict of Interest

The authors declare no conflict of interest.

Keywords

[1] L. Chu, X. Zhang, W. Niu, S. Wu, W. Ma, B. Tang, S. Zhang, *J. Mater. Chem. C* **2019**, *7*, 7411.
[2] S. Beck, J. Bouchard, R. Berry, *Biomacromolecules* **2011**, *12*, 167.
[3] M. Kimura, K. Okahara, T. Miyamoto, *J. Appl. Phys.* **1979**, *50*, 1222.
[4] K. Aslan, M. Wu, J. R. Lakowicz, C. D. Geddes, *J. Am. Chem. Soc.* **2007**, *129*, 1524.
[5] C. J. Orendorff, T. K. Sau, C. J. Murphy, *Small* **2006**, *2*, 636.
[6] R. Yudianti, A. Syampurwadi, H. Onggo, M. Karina, H. Uyama, J. Azuma, *Polym. Adv. Technol.* **2016**, *27*, 1102.
[7] E. F. Gomez, A. J. Steckl, *ACS Photonics* **2015**, *2*, 439.
[8] L. Du, preprint arXiv: 1612.08227, **2016**.
[9] H. Zhu, S. Parvinian, C. Preston, O. Vaaland, Z. Ruan, L. Hu, *Nanoscale* **2013**, *5*, 3787.
[10] M. D. Shawkey, N. I. Morehouse, P. Vukusic, *J. R. Soc., Interface* **2009**, *6*, 221.
[11] M. D. Shawkey, G. E. Hill, *Biol. Lett.* **2005**, *1*, 121.
[12] A. R. Parker, *J. Opt. A: Pure Appl. Opt.* **2000**, *2*, R15.
[13] B. J. Glover, H. M. Whitney, *Ann. Bot.* **2010**, *105*, 505.
[14] S. L. Burg, A. J. Parnell, *J. Phys.: Condens. Matter* **2018**, *30*, 413001.
[15] L. D'Alba, L. Kieffer, M. D. Shawkey, *J. Exp. Biol.* **2012**, *215*, 1272.
[16] D. Gur, Y. Politi, B. Sivan, P. Fratzl, S. Weiner, L. Addadi, *Angew. Chem. Int. Ed.* **2013**, *52*, 388.
[17] H. Simon, *The Splendor of Iridescence*, Vol. 1, Dodd, Mead & Company, New York **1971**.
[18] J. Tinbergen, B. D. Wilts, D. G. Stavenga, *J. Exp. Biol.* **2013**, *216*, 4358.
[19] D. G. Stavenga, J. Tinbergen, H. L. Leertouwer, B. D. Wilts, *J. Exp. Biol.* **2011**, *214*, 3960.
[20] C. Zollfrank, *Scr. Mater.* **2014**, *75*, 3.
[21] R. Schmalensee, T. M. Stoker, R. A. Judson, *Rev. Econ. Stat.* **1998**, *80*, 15.
[22] M. A. Browne, P. Crump, S. J. Niven, E. L. Teuten, A. Tonkin, T. Galloway, R. C. Thompson, *Environ. Sci. Technol.* **2011**, *45*, 9175.
[23] C. Zollfrank, D. Van Opdenbosch, in *Bionanocomposites*, Vol. 1 (Eds: C. Aimé, T. Coradin), John Wiley & Sons, Hoboken, NJ **2017**, Ch. 5.
[24] M. Beckers, B. Weise, S. Kalapis, T. Gries, G. Seide, C.-A. Bunge, in *Polymer Optical Fibres*, Vol. 1 (Eds: C.-A. Bunge, T. Gries, M. Beckers), Woodhead Publishing, Duxford, UK **2017**, Ch. 2.
[25] E. Hecht, *Optics*, Addison Wesley, San Francisco, CA **2002**.
[26] J. T. McNamara, J. L. W. Morgan, J. Zimmer, *Annu. Rev. Biochem.* **2015**, *84*, 895.
[27] D. Klemm, B. Heublein, H. P. Fink, A. Bohn, *Angew. Chem., Int. Ed.* **2005**, *44*, 3358.
[28] H. Staudinger, *Ber. Dtsch. Chem. Ges.* **1920**, *53*, 1073.
[29] T. Heinze, *Adv. Polym. Sci.* **2016**, *271*, 1.
[30] W. Wang, Y. Li, W. Li, B. Zhang, Y. Liu, *Cellulose* **2019**, *26*, 3095.
[31] N. A. El-Wakil, M. L. Hassan, *J. Appl. Polym. Sci.* **2008**, *109*, 2862.
[32] J. A. Cuculo, C. B. Smith, U. Sangwatanaroj, E. O. Stejskal, S. S. Sankar, *J. Polym. Sci., Part A: Polym. Chem.* **1994**, *32*, 229.
[33] K. Hattori, J. A. Cuculo, S. M. Hudson, *J. Polym. Sci., Part A: Polym. Chem.* **2002**, *40*, 601.
[34] M. Hattori, Y. Shimaya, M. Saito, *Polym. J.* **1998**, *30*, 49.
[35] T. R. Dawsey, C. L. McCormick, *J. Macromol. Sci., Phys.* **1990**, *30*, 405.
[36] H. Chanzy, M. Dubé, R. H. Marchessault, *J. Polym. Sci., Polym. Lett. Ed.* **1979**, *17*, 219.
[37] X. Chen, C. Burger, F. Wan, J. Zhang, L. Rong, B. S. Hsiao, B. Chu, J. Cai, L. Zhang, *Biomacromolecules* **2007**, *8*, 1918.
[38] H. Vu-Manh, F. Wendler, H. B. Öztürk, T. Bechtold, *Carbohydr. Polym.* **2012**, *87*, 195.
[39] S. Fischer, H. Leipner, K. Thümmler, E. Brendler, J. Peters, *Cellulose* **2003**, *10*, 227.
[40] Y.-L. Chen, X. Zhang, T.-T. You, F. Xu, *Cellulose* **2019**, *26*, 205.
[41] M. Isik, H. Sardon, D. Mecerreyes, *Int. J. Mol. Sci.* **2014**, *15*, 11922.
[42] J. Sugiyama, R. Vuong, H. Chanzy, *Macromolecules* **1991**, *24*, 4168.
[43] Y. Nishiyama, J. Sugiyama, H. Chanzy, P. Langan, *J. Am. Chem. Soc.* **2003**, *125*, 14300.
[44] L. M. Kroon-Batenburg, J. Kroon, *Glycoconjugate J.* **1997**, *14*, 677.

[45] M. Wada, H. Chanzy, Y. Nishiyama, P. Langan, *Macromolecules* **2004**, *37*, 8548.

[46] K. Hutino, I. Sakurada, *Naturwissenschaften* **1940**, *28*, 577.

[47] M. Wada, L. Heux, J. Sugiyama, *Biomacromolecules* **2004**, *5*, 1385.

[48] J. A. Kelly, M. Giese, K. E. Shopsowitz, W. Y. Hamad, M. J. MacLachlan, *Acc. Chem. Res.* **2014**, *47*, 1088.

[49] J. H. Park, J. H. Noh, C. Schütz, G. Salazar-Alvarez, G. Scalia, L. Bergström, J. P. F. Lagerwall, *Chem. Phys. Chem.* **2014**, *15*, 1477.

[50] J. P. F. Lagerwall, C. Schütz, M. Salajkova, Y. H. Noh, J. H. Park, G. Scalia, L. Bergström, *NPG Asia Mater.* **2014**, *6*, e80.

[51] S. Wang, A. Lu, L. Zhang, *Prog. Polym. Sci.* **2016**, *53*, 169.

[52] T. D. Nguyen, W. Y. Hamad, J. M. MacLachlan, *Chem. Commun.* **2013**, *49*, 11296.

[53] V. Caligiuri, G. Tedeschi, M. Palei, M. Misciuglio, B. Martin-Garcia, S. Guzman-Puyol, M. K. Hedayati, A. Kristensen, A. Athanassiou, R. Cingolani, V. J. Sorger, M. Salerno, F. Bonaccorso, R. Krahne, J. A. Heredia-Guerrero, *ACS Nano* **2020**, *14*, 9502.

[54] R. H. Marchessault, F. F. Morehead, N. M. Walter, *Nature* **1959**, *184*, 632.

[55] J. F. Revol, H. Bradford, J. Giasson, R. H. Marchessault, D. G. Gray, *Int. J. Biol. Macromol.* **1992**, *14*, 170.

[56] A. C. Neville, D. C. Gubb, R. M. Crawford, *Protoplasma* **1976**, *90*, 307.

[57] M. Giese, M. Spengler, *Mol. Syst. Des. Eng.* **2019**, *4*, 29.

[58] C. Schütz, M. Agthe, A. B. Fall, K. Gordeyeva, V. Guccini, M. Salajková, T. S. Plivelic, J. P. F. Lagerwall, G. Salazar-Alvarez, L. Bergström, *Langmuir* **2015**, *31*, 6507.

[59] G. Freymann, V. Kitaev, B. V. Lotsch, G. A. Ozin, *Chem. Soc. Rev.* **2013**, *42*, 2528.

[60] H. L. Vries, *Acta Crystallogr.* **1951**, *4*, 219.

[61] J. Tao, C. Zou, H. Jiang, M. Li, D. Lu, S. Mann, Y. Xu, *CCS Chem.* **2020**, *2*, 932.

[62] A. Tran, W. Y. Hamad, M. J. MacLachlan, *Langmuir* **2018**, *34*, 646.

[63] A. G. Dumanli, G. Kamita, J. Landman, H. van der Kooij, B. J. Glover, J. J. Baumberg, U. Seiner, S. Vignolini, *Adv. Opt. Mater.* **2014**, *2*, 646.

[64] K. Yao, Q. Meng, V. Bulone, Q. Zhou, *Adv. Mater.* **2017**, *29*, 1701323.

[65] X. M. Dong, T. Kimura, J. F. Revol, D. G. Gray, *Langmuir* **1996**, *12*, 2076.

[66] B. Frka-Petesic, G. Guidetti, G. Kamita, S. Vignolini, *Adv. Mater.* **2017**, *29*, 1701469.

[67] Y. Habibi, T. Heim, R. Douillard, *J. Polym. Sci., Part B: Polym. Phys.* **2008**, *46*, 1430.

[68] L. M. Mäthger, E. J. Denton, N. J. Marshall, R. T. Hanlon, *J. R. Soc., Interface* **2009**, *6*, S149.

[69] H. Chen, A. Hou, C. Zheng, J. Tang, K. Xie, A. Gao, *ACS Appl. Mater. Interfaces* **2020**, *12*, 24505.

[70] O. Kose, A. Tran, L. Lewis, W. Y. Hamad, M. J. MacLachlan, *Nat. Commun.* **2019**, *10*, 510.

[71] O. Kose, C. E. Boott, W. Y. Hamad, M. J. MacLachlan, *Macromolecules* **2019**, *52*, 5317.

[72] S. Gazzo, G. Manfredi, R. Pötzsch, Q. Wei, M. Alloisio, B. Voit, D. Comoretto, *J. Polym. Sci., Part B: Polym. Phys.* **2016**, *54*, 73.

[73] D. Yan, R. Li, W. Lu, C. Piao, L. Qiu, Z. Meng, S. Wang, *Analyst* **2019**, *144*, 1892.

[74] A. Espinha, C. Dore, C. Matricardi, M. I. Alonso, A. R. Goñi, A. Mihi, *Nat. Photonics* **2018**, *12*, 343.

[75] D. Yan, L. Qiu, M. Xue, Z. Meng, Y. Wang, *Mater. Des.* **2019**, *165*, 107601.

[76] T. S. Kleine, L. R. Diaz, K. M. Konopka, L. E. Anderson, N. G. Pavlopolous, N. P. Lyons, E. T. Kim, Y. Kim, R. S. Glass, K. Char, R. A. Norwood, J. Pyun, *ACS Macro Lett.* **2018**, *7*, 875.

[77] T. Komikado, A. Inoue, K. Masuda, T. Ando, S. Umegaki, *Thin Solid Films* **2007**, *515*, 3887.

[78] L. E. Anderson, T. S. Kleine, Y. Zhang, D. D. Phan, S. Namnabat, E. A. LaVilla, K. M. Konopka, L. R. Diaz, M. S. Manchester, J. Schwiegerling, R. S. Glass, M. E. Mackay, K. Char, R. A. Norwood, J. Pyun, *ACS Macro Lett.* **2017**, *6*, 500.

[79] G. Manfredi, C. Mayrhofer, G. Kothleitner, D. C. R. Schennach, *Cellulose* **2016**, *23*, 2853.

[80] P. Lova, *Polymers* **2018**, *10*, 1161.

[81] P. Lova, G. Manfredi, L. Boarino, A. Comite, M. Laus, M. Patrini, F. Marabelli, C. Soci, D. Comoretto, *ACS Photonics* **2015**, *2*, 537.

[82] J. R. C. Smirnov, A. Sousaraei, M. R. Osorio, S. Casado, J. J. Hernández, L. Wu, Q. Zhang, R. Xia, D. Granados, R. Wannemacher, I. Rodriguez, J. Cabanillas-Gonzalez, *npj Flex. Electron.* **2019**, *3*, 17.

[83] S. Caixeiro, M. Peruzzo, O. D. Onelli, S. Vignolini, R. Sapienza, *ACS Appl. Mater. Interfaces* **2017**, *9*, 7885.

[84] S. Tadepalli, J. M. Slocik, M. K. Gupta, R. R. Naik, S. Singamaneni, *Chem. Rev.* **2017**, *117*, 12705.

[85] N. Ghofraniha, I. Viola, A. Zacheo, V. Arima, G. Gigli, C. Conti, *Opt. Lett.* **2013**, *38*, 5043.

[86] C. C. Alves, R. Cleber, L. B. Mendonça, J. M. A. Caiut, *J. Mater. Sci.: Mater. Electron.* **2019**, *30*, 16849.

[87] R. Zhang, S. Knitter, S. F. Liew, F. G. Omenetto, B. M. Reinhard, H. Cao, L. Dal Negro, *Appl. Phys. Lett.* **2016**, *108*, 011103.

[88] M. L. da Silva-Neto, M. C. A. de Oliveira, C. T. Dominguez, R. E. M. Lins, N. Rakov, C. B. de Araújo, L. S. Menezes, H. P. de Oliveira, A. S. L. Gomes, *Sci. Rep.* **2019**, *9*, 11765.

[89] I. Viola, N. Ghofraniha, A. Zacheo, V. Arima, C. Conti, G. Gigli, *J. Mater. Chem. C* **2013**, *1*, 8128.

[90] G. C. M. Germano, Y. D. R. Machado, L. Martinho, S. N. Fernandes, A. M. L. M. Costa, E. Pecoraro, A. S. L. Gomes, I. C. S. Carvalho, *J. Opt. Soc. Am. B* **2020**, *37*, 24.

[91] M. Gaio, D. Saxena, J. Bertolotti, D. Pisignano, A. Camposeo, R. Sapienza, *Nat. Commun.* **2019**, *10*, 226.

[92] N. Ghofraniha, L. La Volpe, D. Van Opdenbosch, C. Zollfrank, C. Conti, *Adv. Opt. Mater.* **2016**, *4*, 1998.

[93] R. R. Tummala, *Fundamentals of Microsystems Packaging*, McGraw-Hill Education Ltd., New York **2001**.

[94] A. Gangwar, B. Sharma, *Standard Journal Abbreviation* **2012**, *4*, 19.

[95] P. Kröplin, C. Dieling, M. Beckers, V. Schrank, M. Beer, T. Gries, G. Seide, C.-A. Bunge, in *Polymer Optical Fibres*, Vol. *1* (Eds: C.-A. Bunge, T. Gries, M. Beckers), Woodhead Publishing, Duxford, UK Ch. 11.

[96] M. Large, L. Poladian, G. Barton, M. A. van Eijkelenborg, *Microstructured Polymer Optical Fibres*, Springer, New York **2008**.

[97] O. Polishuk, *IEEE Commun. Mag.* **2006**, *44*, 140.

[98] J. Zubia, J. Arrue, *Opt. Fiber Technol.* **2001**, *2*, 101.

[99] M. Choi, J. W. Choi, S. Kim, S. Nizamoglu, S. K. Hahn, S. H. Yun, *Nat. Photonics* **2013**, *7*, 987.

[100] M. Choi, M. Humar, S. Kim, S. H. Yun, *Adv. Mater.* **2015**, *27*, 4081.

[101] S. Nizamoglu, M. C. Gather, M. Humar, M. Choi, S. Kim, K. S. Kim, S. K. Hahn, G. Scarcelli, M. Randolph, R. W. Redmond, S. H. Yun, *Nat. Commun.* **2016**, *7*, 10374.

[102] A. Gierej, M. Vagenende, A. Filipkowski, B. Siwicki, R. Buczynski, H. Thienpont, S. Van Vlierberghe, T. Geernaert, P. Dubruel, F. Berghmans, *J. Lightwave Technol.* **2019**, *37*, 1916.

[103] D. Shan, C. Zhang, S. Kalaba, N. Mehta, G. B. Kim, Z. Liu, J. Yang, *Biomaterials* **2017**, *143*, 142.

[104] A. Dupuis, N. Guo, Y. Gao, N. Godbout, S. Lacroix, C. Dubois, M. Skorobogatiy, *Opt. Lett.* **2007**, *32*, 109.

[105] H. Orelma, A. Hokkanen, I. Leppänen, K. Kammiovirta, M. Kapulainen, A. Harlin, *Cellulose* **2020**, *27*, 1543.

[106] S. T. Parker, P. Domachuk, J. Amsden, J. Bressner, J. A. Lewis, D. L. Kaplan, F. G. Omenetto, *Adv. Mater.* **2009**, *21*, 2411.

[107] M. B. Applegate, G. Perotto, D. L. Kaplan, F. G. Omenetto, *Biomed. Opt. Express* **2015**, *6*, 4221.

[108] S. Zhang, C. Chen, C. Duan, H. Hu, H. Li, J. Li, Y. Liu, X. Ma, J. Stavik, Y. Ni, *BioResources* **2018**, *13*, 4577.

[109] Q. Yang, H. Fukuzumi, T. Saito, A. Isogai, L. Zhang, *Biomacromolecules* **2011**, *12*, 2766.

[110] X. H. Yang, L. L. Wang, *Opt. Express* **2007**, *15*, 16478.

[111] D. Li, L. Wang, *Opt. Commun.* **2010**, *283*, 2841.

[112] L. Peng, X. Yang, L. Yuan, L. Wang, E. Zhao, F. Tian, Y. Liu, *Opt. Commun.* **2011**, *284*, 4810.

[113] Y. Huang, E. L. Hsiang, M. Y. Deng, S. T. Wu, *Light: Sci. Appl.* **2020**, *9*, 105.

[114] S. Purandare, E. F. Gomez, A. J. Steckl, *Nanotechnology* **2014**, *25*, 094012.

[115] X. Song, S. Yang, X. Liu, M. Wu, Y. Li, S. Wang, *Nanomaterials* **2018**, *8*, 648.

[116] S. Salehifar, M. R. Shayesteh, S. Hashemian, *J. Electron. Mater.* **2018**, *47*, 1279.

[117] G. Z. Abdelmessih, J. M. Alonso, L. Canale, P. Dupuis, A. Alchaddoud, G. Zissis, in *2019 IEEE Int. Conf. on Environment and Electrical Engineering and 2019 IEEE Industrial and Commercial Power Systems Europe (EEEIC/I&CPS Europe)*, IEEE, Genova, Italy **2019**.

[118] E. R. P. Pinto, H. S. Barud, R. R. Silva, M. Palmieri, W. L. Polito, V. L. Calil, M. Cremona, S. J. L. Ribeiro, Y. Messaddeq, *J. Mater. Chem. C* **2015**, *3*, 11581.

[119] C. Legnani, H. S. Barud, J. M. A. Caiut, V. L. Calil, I. O. Maciel, W. G. Quirino, S. J. L. Ribeiro, M. Cremona, *J. Mater. Sci.: Mater. Electron.* **2019**, *30*, 16718.

[120] B. W. Lim, M. C. Suh, *Nanoscale* **2014**, *6*, 14446.

[121] M. Shibano, H. Ochiai, K. Suzuki, H. Kamitakahara, H. Kaji, T. Takano, *Marcomolecules* **2020**, *53*, 2864.

[122] M. Krithikaa, *IJTRD* **2016**, *3*, 74.

[123] G. Walker, *J. Soc. Inf. Disp.* **2012**, *20*, 413.

[124] H. Zhu, Z. Fang, Z. Wang, J. Dai, Y. Yao, F. Shen, C. Preston, W. Wu, P. Peng, N. Jang, Q. Yu, Z. Yu, L. Hu, *ACS Nano* **2016**, *10*, 1369.

[125] S. Ummartyotin, S. Thiangtham, H. Manuspiya, *For. Prod. J.* **2016**, *67*, 288.

[126] S. Ji, B. G. Hyun, K. Kim, S. Y. Lee, S. H. Kim, J. Y. Kim, M. H. Song, J. U. Park, *NPG Asia Mater.* **2016**, *8*, e299.

[127] V. V. Tyagi, N. A. A. Rahim, N. A. Rahim, J. A. L. Selvaraj, *Renewable Sustainable Energy Rev.* **2013**, *20*, 443.

[128] Q. Xu, L. Meng, X. Wang, *Appl. Opt.* **2019**, *58*, 2505.

[129] G. Hou, Y. Liu, D. Zhang, G. Li, H. Xie, Z. Fang, *ACS Appl. Mater. Interfaces* **2020**, *12*, 31998.

[130] B. Parida, S. Iniyan, R. Goic, *Renewable Sustainable Energy Rev.* **2011**, *15*, 1625.

[131] L. Wu, W. Tian, X. Jiang, *Sol. Energy Mater. Sol. Cells* **2005**, *87*, 637.

[132] B. O'Regan, M. Grätzelt, *Nature* **1991**, *353*, 737.

[133] K. Miettunen, J. Vapaavuor, A. Tiihonen, A. Poskela, P. Lahtinen, J. Halme, P. Lund, *Nano Energy* **2014**, *8*, 95.

[134] T. Or, K. Miettunen, E. D. Cranston, J. M. Moran-Mirabal, J. Vapaavuori, *ACS Appl. Energy Mater.* **2019**, *2*, 5635.

[135] A. Chiappone, F. Bella, J. R. Nair, G. Meligrana, R. Bongiovanni, C. Gerbaldi, *ChemElectroChem* **2014**, *1*, 1350.

[136] A. Poskela, K. Miettunen, M. Borghei, J. Vapaavuori, L. G. Greca, J. Lehtonen, K. Solin, M. Ago, P. D. Lund, O. J. Rojas, *ACS Sustainable Chem. Eng.* **2019**, *7*, 10257.

[137] V. Selvanathan, R. Yahya, M. H. Ruslan, K. Sopian, N. Amin, M. Nour, H. Sindi, M. Rawa, M. Akhtaruzzaman, *Polymers* **2020**, *12*, 516.

[138] A. Goetzberger, C. Hebling, H. W. Schock, *Mater. Sci. Eng., R* **2003**, *40*, 1.

[139] B. Azzopardi, C. J. M. Emmott, A. Urbina, F. C. Krebs, J. Mutale, J. Nelson, *Energy Environ. Sci.* **2011**, *4*, 3741.

[140] S. V. Costa, P. Pingel, S. Janietz, A. F. Nogueira, *J. Appl. Polym. Sci.* **2016**, *133*, 43679.

[141] Y. Yao, J. Tao, J. Zou, B. Zhang, T. Li, J. Dai, M. Zhu, S. Wang, K. K. Fu, D. Henderson, E. Hitz, J. Peng, L. Hu, *Energy Environ. Sci.* **2016**, *9*, 2278.

[142] Y. Zhou, C. Fuentes-Hernandez, T. M. Khan, J. C. Liu, J. Hsu, J. W. Shim, A. Dindar, J. P. Youngblood, R. J. Moon, B. Kippelen, *Sci. Rep.* **2013**, *3*, 1536.

[143] L. Nyholm, G. Nyström, A. Mihranyan, M. Strømme, *Adv. Mater.* **2011**, *23*, 3751.

[144] E. Fortunato, N. Correia, P. Barquinha, L. Pereira, G. Gonçalves, R. Martins, *IEEE Electron Device Lett.* **2008**, *29*, 988.

[145] L. J. Gibson, *J. R. Soc., Interface* **2012**, *9*, 2749.

[146] Y. Habibi, L. A. Lucia, O. J. Rojas, *Chem. Rev.* **2010**, *110*, 3479.

[147] R. J. Moon, A. Martini, J. Nairn, J. Simonsen, J. Youngblood, *Chem. Soc. Rev.* **2011**, *40*, 3941.

[148] L. Hu, G. Zheng, J. Yao, N. Liu, B. Weil, M. Eskilsson, E. Karabulut, Z. Ruan, S. Fan, J. T. Bloking, M. D. McGehee, L. Wågberg, Y. Cui, *Energy Environ. Sci.* **2013**, *6*, 513.

[149] L. La Notte, P. Cataldi, L. Ceseracciu, I. S. Bayer, A. Athanassiou, S. Marras, E. Villari, F. Brunetti, A. Reale, *Mater. Today Energy* **2018**, *7*, 105.

[150] D. E. Smalley, E. Nygaard, K. Squire, J. Van Wagoner, J. Rasmussen, S. Gneiting, K. Qaderi, J. Goodsell, W. Rogers, M. Lindsey, K. Costner, A. Monk, M. Pearson, B. Haymore, J. Peatross, *Nature* **2018**, *553*, 486.

[151] E. J. Davis, *Aerosol Sci. Technol.* **1997**, *26*, 212.

[152] W. Rogers, J. Laney, J. Peatross, D. Smalley, *Appl. Opt.* **2019**, *58*, G363.

[153] R. Service, *Science* **2003**, *301*, 909.

[154] M. Ebner, R. Schennach, H. T. Chien, C. Mayrhofer, A. Zankel, B. Friedel, *Flexible Printed Electron.* **2017**, *2*, 014002.

Martin Reimer is a Ph.D. candidate in the biogenic polymers group at the Technical University of Munich under the supervision of Prof. Cordt Zollfrank. He holds a M.Sc. degree in "Renewable Resources" from the TUM Campus Straubing for Biotechnology and Sustainability. His research interests are focused on the design and synthesis of novel bioinspired and biopolymer optical fibers.

Cordt Zollfrank studied chemistry at Technical University of Munich (TUM), where he gained a Ph.D. in forest sciences. He subsequently worked as a postdoctoral research fellow at the University of Erlangen-Nuremberg (2000–2002) conducting research focused on biomimetic material synthesis. 2002 he became a group leader and set up a bioengineered ceramics and biomaterials research group. He acquired his teaching qualification (habilitation) in material sciences in 2009. In 2011, he accepted the position as Associate Professor for Biogenic Polymers at the TUM Campus Straubing for Biotechnology and Sustainability and was recently promoted to Full Professor for Biogenic Polymers in 2020.